Catestatin (CST) is a key mediator of the immunoendocrine regulation of cardiovascular function

Wei Ying[2*], Kechun Tang[1*], Ennio Avolio[2#], Jan M. Schilling[1,3], Teresa Pasqua[2#], Matthew A. Liu[2], Hongqiang Cheng[4], Jing Zhang[2], Sumana Mahata[2], Gautam Bandyopadhyay[2], Soumita Das[5], David M. Roth[1,3], Debashis Sahoo[6,7], Nicholas J.G. Webster[1,3], Farah Sheikh[2], Hemal H. Patel[1,3] Pradipta Ghosh[1,2,8] and Sushil K. Mahata[1,2¶].

[1]VA San Diego Healthcare System, 3350 La Jolla Village Drive, San Diego, CA, USA

[2]Department of Medicine, [3]Anesthesiology, [5]Pathology, [6]Pediatrics, [7]Department of Computer Science and Engineering, [8]Cellular and Molecular Medicine, University of California San Diego, La Jolla, CA, USA

[4]Department of Cardiology, Sir Run Shaw Hospital, Zhejiang University School of Medicine, Hangzhou, China

[#]Present address: Department of Biology, University of Calabria, Rende, CS, Italy

*Contributed equally to this work.

¶Correspondence should be addressed to: Sushil K. Mahata, Metabolic Physiology & Ultrastructural Biology Laboratory, Department of Medicine, University of California San Diego, 9500 Gilman Drive, La Jolla, CA 92093-0732, smahata@health.ucsd.edu.

Abstract

Hypertension is a global pandemic, affecting more than one billion people. We generated CST knockout (CST-KO) mice to pinpoint the role of CST in hypertension. CST-KO mice are hypertensive and display left ventricular hypertrophy. Serum cytokines are elevated and their hearts show marked infiltration with macrophages. CST replenishment reverses these phenotypes. Pre-conditioning-induced cardioprotection is also abolished in CST-KO mice. CST-KO mice became normotensive when given chlodronate to deplete macrophages or when given bone marrow from wild-type littermates, implicating macrophage regulation of the hypertensive phenotype in CST-KO mice. Cardiac tissue transcriptomes revealed altered gene expression in CST-KO mice that are similar to human cardiomyopathies. For example, a reduction of *Glo1* was seen in CST-KO mice, while CST supplementation increased its expression. Because *Glo*1 in macrophages metabolizes methylglyoxal, an inflammatory agent linked to vascular damage in hypertension and diabetes, increasing expression with CST may attenuate inflammation and improve cardiovascular health. Repletion of CST also increased glucose metabolism and decreased catecholamine secretion; the latter explains CST's anti-hypertensive action. The anti-hypertensive effects of CST are mediated at least partly via CST's anti-inflammatory actions. The findings also implicate CST as a key mediator of the observed crosstalk between systemic and cardiac inflammation in hypertension.

Nonstandard Abbreviations and Acronyms

2DG, 2-deoxy-glucose
Actc1, cardiac muscle actin alpha
Ang4, angiogenin ribonuclease family member 4
Arg1, arginase 1
Astn2, astrotactin 2
ATP, adenosine triphosphate
Atp5j, mitochondrial ATP synthase subunit F6
BMT, bone-marrow transplantation
BP, blood pressure
Cap1, adenylate cyclase-associated protein 1
Ccl2 (Mcp1), chemokine CC motif ligand 2
CDN, chlodronate
Cd36, cluster of differentiation 36
Cers2, ceramide synthase 2
CgA, chromogranin A
Clec7a, C-type lectin family domain 7, member A
Clec10a, C-type lectin family domain 10, member A
Col1a2, collagen type 1 alpha 2
CST, catestatin
CST-KO, CST knockout
Cyb5, cytochrome b5
DA, dopamine
Defa20, defensin a-20
DIO, diet-induced obese
Dgat2, diacylglycerol O-acyltransferase 2
Ear11, eosinophil-associated ribonuclease A family member 11
Emr1 (F4/80), epidermal growth factor-like module containing mucin-like hormone receptor 1
EPI, epinephrine
FA, fatty acid
FACS, fluorescence activated cell sorting
FRT, *Flp* recognition target
G6P, glucose-6-phosphate
Glo1, glyoxylase I
Glut4, glucose transporter 4
Gm7120, predicted gene 7120
GSK-3β, glycogen synthase kinase-3 beta
HTN, hypertension
IACUC, institutional animal care and use committees
IFM, inter/intramyofibrillar mitochondria
Il2, interleukin 2
Il4, interleukin 4
Il6, interleukin 6
Il10, interleukin 10

IPC, ischemic preconditioning
IFNγ, interferon gamma
Il12p40, interleukin 12 subunit p40
Itgam (Cd11b), integrin alpha-M
Itgax (Cd11c), integrin alpha-X
Kc/Gro, keratinocyte chemoattractant/growth related oncogene
KOH, potassium hydroxide
LVDP, left ventricular developed pressure
LVEDP, left ventricular end diastolic pressure
mAb, monoclonal antibody
Mip1α, macrophage inflammatory protein 1 alpha
Mrc1, macrophage mannose receptor 1
Myl4, myosin light chain 4
Myl7, myosin light chain 7
Myh7, myosin heavy chain 7
NADH, nicotinamide adenine dinucleotide hydride
NCD, normal chow diet
NE, norepinephrine
Nos2a (Inos), nitric oxide synthase 2A
Nppa, natriuretic peptide precursor A
pAb, polyclonal antibody
Pam, peptidylglycine alpha-amidating monooxygenase
Pdk2, pyruvate dehydrogenase kinase 2
Pfkm, phosphofructokinase, muscle form
PI-3K, phosphoinositide 3-kinase
Pparα: peroxisome proliferator-activated receptor alpha
qPCR, quantitative polymerase chain reaction
ROS, reactive oxygen species
SBP, systolic blood pressure
Sdhc, succinate dehydrogenase complex subunit c
Slc27a1, solute carrier family 27 member 1
Slc27a2, solute carrier family 27 member 2
SNA, sympathetic nerve activity
Sptlc1, serine palmitoyltransferase long-chain base subunit 1
SSM, subsarcolemmal mitochondria
T2DM, Type 2 diabetes mellitus
TCA, trichloroacetic acid
TEM, transmission electron microscopy
TNFα, tumor necrosis factor alpha
Tnni3, cardiac Troponin I
Tnnt2, cardiac Troponin T2
Tpm, tropomyosin
Ttn, Titin

146 **Introduction**

147 Hypertension (HTN) is an important risk factor for cardiovascular disease (CVD) and
148 mortality (1). The burden of HTN and the estimated HTN-associated deaths have
149 increased substantially over the past 25 years.

150 The role of catecholamines, e.g., dopamine (DA), norepinephrine (NE), and
151 epinephrine (EPI) in the regulation of blood pressure (BP) and their dysregulated
152 secretion or function in HTN has been well recognized (2, 3). Catecholamines are
153 produced and secreted predominantly by chromaffin cells in the adrenal medulla and
154 have hormonal and neurotransmitter functions. Once released, catecholamines interact
155 with adrenergic receptors to impose an intricate neuro-hormonal regulation of BP.

156 Besides catecholamines, the immune system is also recognized for the genesis
157 and progression of HTN(4, 5). Inflammation is an essential component of many diseases,
158 and the connections between innate and adaptive immunity, HTN and CVD support the
159 role of the immune system in cardiovascular pathology (5). Known as integrators of
160 neural, hormonal, and immune signals, inflammation influences catecholamine
161 biosynthesis. The converse, how catecholamines may impact inflammation, remains
162 unknown. More specifically, although the impact of immune activation and inflammation
163 in the regulation of HTN is evolving, the specific immunologic mechanisms that contribute
164 to the pathogenesis of HTN are incompletely understood. Here we reveal an unexpected
165 finding of how the process of catecholamine secretion and its impact on systemic HTN is
166 fueled by an immunologic phenomenon *via* Chromogranin A (CgA), and more specifically,
167 its proteolytic biologic fragment, catestatin (CST: $hCgA_{352-372}$) (6).

168 Co-stored and co-released with catecholamines, CgA, a ~49 kDa secretory
169 proprotein, (7, 8) is overexpressed in humans with essential HTN (9) and in rodent
170 genetic models of HTN (10). Unlike CgA, plasma CST levels are diminished not only in
171 essential HTN (9, 11) but also in the normotensive offspring of patients with HTN (11).
172 Additionally, HTN-associated single nucleotide polymorphisms within the CST segment
173 of CgA have been extensively evaluated (12-15). Processing of CgA to CST is low in
174 patients with HTN and heart failure (9, 16), suggesting dysregulation in the processing of
175 CgA to CST in CVD. Furthermore, both CgA heterozygote (CgA+/-) and CgA knockout
176 (CgA-/-) mice are hypertensive (17); but treatment with CST decreases BP and the levels

177 of plasma catecholamines to that seen in control littermates. Although these findings,
178 especially the repletion studies, point to the importance of CST and its sufficiency in
179 reversing HTN, none conclusively show that CST is necessary. This is because CgA has
180 many biologically active peptides (18), and it is possible that any or many of these CgA-
181 derived peptides could be confounding the findings in these studies.

182 To mitigate these issues, and pinpoint the actions of CST, we generated a precise
183 tool, i.e., CST-KO mice. Given the hypertensive, hyperadrenergic, and inflammatory
184 phenotypes in these mice, we used that as a model to dissect the role of CST in the
185 maintenance of cardiovascular homeostasis. Our studies revealed a complex interplay
186 between a trifecta: the innate immune system, the adrenal medulla with its catecholamine
187 secretion catecholamine secretion and the cardiovascular system, all coordinated by
188 CST.
189
190

Results

Generation and validation of CST-KO mice. Our strategy (see **Fig 1; S1A**) for the development of CST-KO mice involved a targeted elimination of the CST domain (63 bp) from Exon VII of the *Chga* gene. Using a mouse monoclonal antibody (mAb 5A8), we detected full-length CgA (~70 kDa) in WT mice and a proteoglycan form of CgA in CST-KO mice in adrenal gland lysates (**Fig. 1B**), indicating the presence of CgA in CST-KO mice. However, blots using a polyclonal antibody directed against the C-terminal domains of CST (pAb CT-CST) showed a proteolytically processed CgA (~46 kDa) corresponding to $mCgA_{1-385}$ in WT littermates, but not in CST-KO mice (**Fig. 1C**). Because this antibody detected synthetic CST (a positive control, indicating specificity of the antibody) we conclude that CST-KO mice indeed lack CST (**Fig. 1C**). Adrenal CgA content was comparable in WT and CST-KO mice (**Fig. 1D**), confirming expression of CgA in CST-KO mice. Plasma CST levels further confirmed the complete absence of CST in CST-KO mice (**Fig. 1E**).

CST-KO mice are hypertensive and show thickened left ventricular posterior wall. To test whether lack of CST affected heart structure and function, we undertook echocardiographic ultrasound imaging, as it provides a comprehensive array of information on cardiac anatomy, physiology, and mechanical properties. The findings revealed that although CST-KO mice maintained a similar level of left ventricular function (fractional shortening) to age-matched WT mice, there were significant abnormalities in LV remodeling as evidenced by the significant increase in LV posterior wall thickness (LVPWd) and a mild increase in interventricular septum wall thickness (IVSd) ($p=0.07$) when compared to WT control mice (**Fig. 1J-L**). Heart rate (HR), fractional shortening, left ventricular internal diameter during systole (LVIDs) and left ventricular internal diameter during diastole were comparable between WT and CST-KO mice (Fig. S1B-E). Consistent with echocardiography findings, CST-KO mice showed increased heart weights coupled with enlarged hearts compared to WT mice (**Fig. 1F&G**). Consistent with the association between increased posterior wall thickness with high BP (19-22), we found that the CST-KO mice are hypertensive (**Fig. 1H**). These findings indicate that CST regulates heart structure and function.

222 Next, we checked plasma CST levels. In WT mice, the plasma CST level was 0.86
223 nM, which increased to 1.72 nM 24 hr after intraperitoneal treatment with CST (2 μg/g
224 body weight) (**Fig. 2A&B**). In CST-KO mice, plasma CST was undetectable at baseline,
225 as expected, and rose to 1.17 nM after 24 hr of CST supplementation (**Fig. 2B**), indicating
226 that CST supplementation provided a near physiological concentration of CST. We next
227 examined the CST-KO phenotypes and asked whether CST supplementation can restore
228 some of the key phenotypes.
229 First, we found that CST-KO mice show increased levels of proinflammatory
230 plasma cytokines, including TNFα, IFNγ, MIP1α, MCP1, and KC/GRO (**Fig. 2C**). By
231 contrast, the anti-inflammatory cytokine IL10 was decreased in CST-KO mice (**Fig. 2C**).
232 CST treatment decreased proinflammatory cytokines and increased anti-inflammatory
233 cytokines in both WT and CST-KO mice (**Fig. 2C**), which were consistent with transcripts
234 in the heart muscle. CST-KO mice showed a reduction in several anti-inflammatory
235 markers (*IL4*, *Arg1*, *Clec7a* and *Clec10a*) (**Fig. 2D**) and a concomitant increase in several
236 other pro-inflammatory markers (**Fig. 2E**). These findings show that the balance between
237 pro- and anti- inflammatory pathways is skewed towards inflammation in CST-KO mice.
238 CST supplementation (2 μg/g BW for 15 days) reversed this disbalance; it induced several
239 anti-inflammatory pathways (**Fig. 2D**) and either normalized or markedly decreased
240 proinflammatory cytokine mRNA levels (**Fig. 2E**). These findings show that CST is both
241 necessary and sufficient for restoring immune homeostasis in accordance with CST's role
242 as an anti-inflammatory peptide (23-26).
243 Second, we checked the systolic BP (SBP) in these mice: high BP in CST-KO mice
244 was reduced to WT level after supplementation with CST (**Fig. 3A-B**), demonstrating that
245 CST is necessary and sufficient for BP homeostasis. This is consistent with the anti-HTN
246 functions of CST (17, 27). In addition, the proinflammatory hypertensive phenotype in
247 CST-KO mice is also consistent with prior studies showing that proinflammatory cytokine
248 (IL6) increases BP (28, 29) and anti-inflammatory cytokines (IL2 and IL10) decrease BP
249 (30-32).
250 Third, we analyzed the microarchitecture of the heart: In the saline-treated WT
251 mice, Transmission Electron Microscopic (TEM) micrographs showed resident
252 macrophages in the inter-sarcolemmal spaces (**Fig. 3C**). In contrast, the saline-treated

253 CST-KO heart showed a marked infiltration of monocyte-derived macrophages (**Fig. 3C**),
254 indicating inflammation of the CST-KO heart; other immune cells, e.g., neutrophils and
255 lymphocytes, constitute <15% of all immune cells observed (**Fig. S4**). While treatment of
256 WT mice with CST did not change the resident macrophage population, CST-KO mice
257 showed almost complete disappearance of infiltrated macrophages after CST substitution
258 (**Fig. 3F**). This was supported by FACS analysis showing ~38% decrease of
259 $CD11b^{+}F4/80^{+}$ macrophages in CST-supplemented CST-KO heart (**Fig. 3D**), revealing
260 that CST is required for cardiac homeostasis and its absence is permissive to cardiac
261 inflammation. Consistent with macrophage-induced fibrosis, CST-KO heart displayed
262 marked cardiac fibrosis as shown by Masson's trichrome staining (**Fig. S3A&B**) and TEM
263 micrographs (**Fig S3C-G**). Fibrosis was markedly reduced upon supplementation of CST-
264 KO mice with CST (**Fig. S3F**).
265
266 **Macrophages are key effector cells responsible for the anti-inflammatory actions**
267 **of CST.** Next, we explored the implications of infiltrated macrophages in the CST-KO
268 hearts and its relevance to cardiovascular physiology using two independent approaches
269 (**Fig. 3A**). First, we depleted macrophages by chlodronate (CDN) liposomes (**Fig. S4B-**
270 **E**), which not only depleted resident and infiltrated macrophages but also reversed the
271 HTN phenotype of CST-KO mice (**Fig. 3G&H**). Gating strategy is shown in **Fig. S4A**.
272 Because CDN did not reduce BP in WT mice, these findings show that macrophages may
273 not be required for normal cardiac functions, but its dysregulation (increased infiltration
274 and/or aberrant activation) may be a key contributor of the HTN phenotype in CST-KO
275 mice.
276 Second, we carried out bone marrow (BM) transplantation (BMT) assays in which
277 we irradiated both WT and CST-KO mice and then cross-transplanted their marrows -
278 CST-KO-BM was transplanted into WT mice and *vice versa*. To our surprise, we found
279 that BMT could transfer the hypertensive phenotype - while CST-KO-BM recipient WT
280 mice showed increased BP, WT-BM recipient CST-KO mice showed decreased BP (**Fig.**
281 **3I**), indicating that paracrine secretion of CST and/or cytokines by macrophages may
282 regulate BP.

283 To confirm whether CST is responsible for the observed BMT-induced phenotype
284 switch, we analyzed plasma CST and found that WT-BM recipient CST-KO mice, but not
285 CST-KO-BM recipients, had near physiologic levels of plasma CST (0.52 nM) (**Fig. 3J**),
286 suggesting that marrow-resident immune cells and/or hematopoietic system are
287 significant contributors of circulating CST. They may do so either directly through
288 paracrine secretion from macrophages, as observed in the case of serum cytokines (**Fig.**
289 **2C**) or indirectly (perhaps *via* other immune cells that feedback and regulate macrophage
290 response).
291 Regardless, our studies using CDN and BMT implicate the macrophages and the
292 innate immune system as key effectors of the anti-hypertensive actions of CST. In the
293 absence of CST (as in CST-KO mice), macrophages are hyperactive and support both
294 systemic (**Fig. 2**) and local cardiovascular inflammation (**Fig. 3**) and trigger systemic HTN.
295
296 **Microarray studies reveal that CST impacts core bioenergetic and metabolic**
297 **functions of the myocardium.** To gain insight into the nature of the immunoendocrine
298 actions of CST on the heart, we carried out transcriptomic analyses of the left ventricle
299 (LV) (gene microarray) in WT and CST-KO mice, which revealed 437 genes with altered
300 expression, up- or downregulated (false discovery rate <0.05), as shown in the form of a
301 heatmap (**Fig. 4A**).
302 Downregulated genes, which were most enriched in pathways that impact muscle
303 conduction and contractility (**Fig. 4B**) include, among other genes, *Glo1* (detoxifies
304 methylglyoxal, which is a cytotoxic byproduct of glycolysis). Upregulated genes include
305 *Gm7120* (acts as a hypercapnia responsive gene), *Astn2* (functions as a lipid raft), and
306 *Defa20* (exerts antibacterial humoral response) genes.
307 We validated several of these up- and downregulated genes by qPCR and found
308 that CST supplementation reversed these aberrant expressions in all cases, i.e.,
309 downregulated what was aberrantly overexpressed or upregulated what was aberrantly
310 suppressed (**Fig. 4C**). Of note, *Glo1* in macrophages metabolizes methylglyoxal, an
311 inflammatory agent whose accumulation promotes vascular damage in HTN and
312 diabetes. Therefore, it is possible that CST attenuates inflammation and improves
313 cardiovascular health in part through the regulation of *Glo1* expression.

314 Targeted qPCR analyses of sarcomeric genes revealed reduced expression of
315 *Tnni3* (coordinates the contraction of the heart), *Tnnt2* (coordinates cardiac contraction),
316 *Myl4* (modulates atrial fibrillation) and *Myl7* (modulates cardiac development and
317 contractility) genes in CST-KO mice (**Fig. 4D**). CST treatment increased expression of
318 *Tnni3*, *Tnnt2*, *Actc1* (regulates cardiomyopathy), *Myl4* and *Myl7* genes in both WT and
319 CST-KO mice albeit to a much higher level in CST-KO mice (**Fig. 4D**).
320 *Tpm* (regulates cardiac contraction) and *Ttn* (regulates cardiac contraction) genes
321 were not affected by the presence or absence of CST.
322 An analysis of mitochondrial genes revealed reduced expression of *Ndufa3*
323 (modulates the transfer of electrons from NADH to the respiratory chain in complex I),
324 *Sdhc* (regulates electron transfer from succinate to ubiquinone in Complex II) and *Atp5j*
325 (produces ATP from ADP in Complex V) genes in CST-KO mice (**Fig. 4E**). CST treatment
326 increased the expression of all three genes in WT and CST-KO mice (**Fig. 4E**).
327 Taken together, these unbiased approaches and qPCR validation studies provide
328 insight into how an inflamed dysfunctional CST-KO heart may impact core fundamental
329 functions by affecting its ultrastructure, muscle function (contractility), rhythm,
330 mitochondrial bioenergetics and conduction.
331
332 **CST-KO mice display a cardiometabolic shift: glucose utilization is decreased with**
333 **a concomitant increase in the utilization of fatty acids and insulin resistance.** We
334 next asked how CST may impact metabolism. The heart is an omnivore, consuming fat,
335 carbohydrate, protein, ketone bodies, or lactate (33), and generating ~95% of total energy
336 via oxidation of fatty acids (FA) and glucose (34). Because diabetic hearts shift away from
337 the utilization of glucose (35), relying almost completely on FA as an energy source, we
338 looked at cardiac metabolism in insulin-resistant CST-KO mice (23). CST-KO mice
339 showed decreased uptake of 2DG in LV compared to WT mice (**Fig. 5A**). Furthermore,
340 G6P utilization was significantly lower in CST-KO compared to WT (**Fig. 5A**). G6P
341 formation was not altered in CST-KO mice (**Fig. 5A**).
342 We next looked at the mRNA levels of key genes involved in glucose metabolism.
343 Thus, we found decreased mRNA expressions of *Glut4* (transports glucose into cell),
344 *Pfkm* (catalyzes the irreversible conversion of fructose-6-phosphate to frustose-1,6-

345 bisphosphate) and *Pdk2* (inhibits pyruvate dehydrogenase activity resulting in decreased
346 glucose utilization and increased fat metabolism) in CST-KO mice compared to WT mice
347 (**Fig. 5B**), which corroborates with the biochemical findings.

348 Poor glucose metabolism in CST-KO mice is consistent with its reduced insulin
349 sensitivity (23). CST supplementation improved glucose uptake, G6P formation and
350 utilization in CST-KO mice (**Fig. 5A**), indicating CST has an insulin-like activity or CST is
351 an insulin-sensitizing peptide. We also found that compared to WT mice, CST-KO mice
352 show a significantly higher FA uptake (**Fig. 5C**) due to the higher plasma insulin level in
353 CST-KO mice, (23) which drives increased lipid metabolism. Furthermore, ^{14}C-labeled
354 acid soluble metabolites (ASM) were significantly higher in CST-KO compared to WT
355 mice (**Fig. 5C**), suggesting that increased dependence on FA for energy needs make
356 CST-KO hearts resistant to insulin.

357 We confirmed these biochemical findings by analyzing the levels of expression of
358 key genes involved in lipid metabolism. We found increased mRNA levels of FA
359 transporter *Cd36* (functions in high affinity tissue uptake of long-chain FA) and *Slc27a1*
360 *(FATP1)* (transports long-chain FA) as well as of the enzyme for triglyceride formation
361 *Dgat2* (catalyzes the terminal step in triacylglycerol synthesis), and the transcription factor
362 *Pparα,* which supports FA oxidation (**Fig. 5D**). In addition, we found increased expression
363 of *Sptlc1* (catalyzes the 1st step in sphingolipid biosynthesis) and *Cers2* (catalyzes the
364 synthesis of very long acyl ceramides) genes (**Fig. 5D**), indicating increased ceramide
365 synthesis, which will make the CST-KO heart more resistant to insulin.

366 In contrast, CST treatment decreased expression of *Cd36*, *Dgat2*, *Sptl1c*, *Cers2*
367 and *Pparα* genes (**Fig. 5D**), indicating that CST improved metabolic health of the CST-
368 KO heart by making them insulin-sensitive. Next, we checked the status of glycogen. We
369 found low glycogen storage in 'Fed' CST-KO heart compared to 'Fed' WT mice. CST
370 supplementation improved glycogen storage in both WT and CST-KO heart as evidenced
371 by biochemical and ultrastructural analyses (**Fig. 5E-G**).

372 Furthermore, because increased accumulation of FA, diacylglycerol, and ceramide
373 impairs insulin signaling (36), we also evaluated WT and CST-KO hearts for
374 phosphoproteins (e.g., AKT and GSK-3β) crucial for insulin signaling. We found that the
375 CST-KO hearts had reduced phosphorylation of AKT at ser473 site and GSK-3β at ser9

site (**Fig. 5H-J**), indicating decreased insulin sensitivity. This phenotype was reversed upon CST treatment (**Fig. 5H-J**), reinforcing CST as an insulin-sensitizing peptide in the heart, which is consistent with previous studies in liver (23, 37).

Taken together with the cardiometabolic shifts, these findings indicate that CST maintains cardiometabolic homeostasis; it does so at least in part by acting as an insulin-sensitizing peptide, thereby allowing the heart to use glucose for generating ATP.

The myocardium in CST-KO mice show mitochondrial dysfunction. The myocardium relies heavily on mitochondria for the generation of ATP and maintenance of intracellular Ca^{2+} fluxes (38). HTN is associated with structural mitochondrial abnormalities that result in impaired energy production and accelerated formation of reactive oxygen species (ROS) through instability of electron transport chain complexes (39). Because the hypertensive CST-KO mice showed gene expression **(Fig. 4)** and biochemical **(Fig. 5)** profiles indicative of altered bioenergetics and mitochondrial dysfunction, next we analyzed the mitochondria health in the WT and CST-KO mice. To this end, we used TEM to analyze and resolve the two populations of mitochondria in the heart - the intermyofibrillar mitochondria (IFM) which align in longitudinal rows between myofibrils and the subsarcolemmal mitochondria (SSM) that localize below the sarcolemma. These two subpopulations have distinct respiration rates associated with different metabolic enzyme activities, morphological structures, and lipid contents (40, 41). Under low magnification we analyzed the shape, location and orientation of SSM (**Fig. 6A-D**) and IFM (**Fig. 6I-L**). Under high magnification we analyzed the shape and orientation of mitochondrial cristae [SSM (**Fig. 6E-H**) and IFM (**Fig. 6M-P**)]. These morphometric analyses revealed significant reduction in cristae surface area in CST-KO mice, which was rescued after CST supplementation (**Fig 6E-H; 6M-P**).

Because cristae shape and density determine the assembly and stability of respiratory chain supercomplexes and efficiency (39), taken together with transcriptomic and biochemical analyses the TEM findings showed that both mitochondrial structure and function are impaired in the hearts of CST-KO mice.

Consistent with myocardial insulin resistance, CST-KO hearts showed accumulation of lipid droplets (**Fig. 6K**), which are implicated in contractile and diastolic

407 dysfunctions (42). Mitophagy, the mitochondrial-specific analog of autophagy, represents
408 breakdown of damaged and malfunctioning mitochondria (43). Ultrastructural
409 demonstration of mitophagy in CST-KO mice (**Fig. 6C&R**) indicates impaired
410 mitochondrial function. CST supplementation improved cristae surface area (**Fig. 6S**),
411 markedly reduced lipid accumulation (**Fig. 6L**), and decreased mitophagy in CST-KO
412 heart (**Fig. 6D**), indicating that CST can enhance cardiovascular functions by improving
413 mitochondrial health and thus cardiomyocyte metabolism.
414
415 **Ischemic pre-conditioning-induced cardioprotection is severely impaired in CST-**
416 **KO heart.** We subjected WT and CST-KO hearts to ischemia/reperfusion (I/R) followed
417 by ischemic preconditioning (IPC). Assessing 'LVDP (mmHg)' (**Fig. S5A**), 'LVEDP
418 (mmHg)' (**Fig. S5C**), 'dP/dt$_{max}$ (mmHg/sec.)' (**Fig. S5B**), 'dP/dt$_{min}$ (mmHg/sec.)' (**Fig. S5D**)
419 revealed that IPC significantly increased post-ischemic LVDP and lowered LVEDP in WT
420 hearts compared to CST-KO hearts and their respective IR controls (**Fig S5A&5C**).
421 Furthermore, neither LVDP nor LVEDP was significantly modified in IPC-treated CST-KO
422 hearts compared to respective IR controls. IPC improved recoveries of both dP/dt$_{max}$ (**Fig.**
423 **S5C**) and dP/dt$_{min}$ (**Fig. S5D**) compared to respective IR controls. When compared to
424 CST-KO mice, a moderate effect on dP/dt$_{max}$ and dP/dt$_{min}$ was seen. Furthermore, neither
425 dP/dt$_{max}$ nor dP/dt$_{min}$ was increased significantly in IPC treated CST-KO hearts compared
426 to respective IR controls.
427 In aggregate, these data show CST-KO mice could not be preconditioned to the
428 extent seen in WT mice. WT mice were protected with IPC, with observed improvements
429 in all functional measures in the reperfusion period, while CST-KO mice showed only
430 marginal improvements.
431
432 **CST-KO adrenal medulla is populated with infiltrated macrophages and fibrosis**
433 **coupled with heightened sympathetic stimulation and hypersecretion of**
434 **catecholamines.** Because prior studies have implicated altered catecholamine secretion
435 from an inflamed adrenal medulla in progression of HTN (2, 3), we evaluated CST-KO
436 adrenal glands. TEM studies revealed abundant infiltration of macrophages and fibrosis
437 in the intercellular spaces of chromaffin cells in CST-KO mice (**Fig. 7A and S6)**. CST

438 supplementation reduced the abundance of macrophage infiltrates in CST-KO mice, but
439 did not affect the resident macrophage population in the WT mice (**Fig. 7A**). By contrast,
440 treatment with CDN resulted in complete loss of macrophages (both resident and
441 infiltrates) in both WT and CST-KO mice (**Fig. 7A**).

442 Because prior studies in humans, mice, and rats have shown that pro-inflammatory
443 cytokines such as IFNα (44), IL1β (45), and TNFα(46) increase catecholamine production
444 and secretion, we wondered if the inflamed CST-KO adrenal glands produce and secrete
445 more catecholamines. We found that compared to WT littermates, both adrenal and
446 plasma catecholamine levels were elevated in CST-KO mice (**Fig. 7B&C**). In addition,
447 the CST-KO adrenal medulla exhibit abundant docked chromaffin granules and
448 decreased acetylcholine containing vesicles at the sympatho-adreno-medullary synapse
449 (**Fig. 7D&E**), implicating heightened sympathetic nerve activity (SNA) eventuating in
450 hypersecretion of catecholamines. Supplementation of CST-KO mice with CST not only
451 inhibited infiltration of macrophages in the adrenal medulla (**Fig. 7A**) but also had a
452 concomitant decrease in both plasma and adrenal catecholamines (**Fig 7B&C**).

453 These findings demonstrate that CST is necessary and sufficient to suppress
454 catecholamine production and secretion and thereby exert an anti-HTN effect and
455 orchestrate cardiometabolic homeostasis. Findings also support the following working
456 model for how CST may accomplish these roles *via* two independent but synergistic
457 mechanisms (see **Fig. 8**): (i) inhibiting the infiltration of macrophages, thereby inhibiting
458 paracrine cytokine regulation of catecholamine production and secretion, (ii) attenuating
459 SNA, thereby decreasing cholinergic stimulus for secretion of catecholamines.
460
461
462

463 **Discussion**
464

465 Previous studies showing low levels of CST in hypertensive subjects (11) and
466 normalization of BP in CgA-KO mice by CST (17) as well as decreasing BP in rodent HTN
467 (27) indicate that CST is sufficient to reverse HTN. The findings of hypertensive
468 phenotype in CST-KO mice and restoration of that phenotype by exogenous
469 administration of recombinant CST establishes that CST is both necessary and sufficient
470 in regulating HTN. This precise experimental model also uncovered three mutually
471 interdependent mechanisms (discussed below) by which CST may exert its anti-HTN and
472 cardioprotective effects and therefore maintain cardiovascular homeostasis.
473

474 **Immunoendocrine regulation of BP.** Cardiac macrophages are critical for myocardial
475 homeostasis (47, 48). While a subset of macrophages orchestrate monocyte recruitment
476 and contribute to heart failure pathogenesis (49), others are increased during diastolic
477 dysfunction (50), myocardial infarction, and acute hemodynamic stress (51). We found
478 an abundance of infiltrated macrophages in the hearts and the adrenal glands of CST-
479 KO mice. Using two parallel approaches (CDN and BMT) to decrease macrophage
480 activity, we found that macrophages are key effector cells for the anti-HTN actions of
481 CST.
482

483 **Immune regulation of cardiometabolic homeostasis, mitochondrial structure and**
484 **function.** The regulation of heart function by immune cells is well documented (52).
485 Although myocardial dysfunctions in rodents (53) and humans (54) have been associated
486 with increased TNFα production, how inflammation may reduce cardiac contractility
487 and/or conduction, two of the most important functions of the myocardium, remains poorly
488 defined. Contractility of the myocardium requires ATP (55), ~6 kg of ATP/ d, which is ~20
489 times its own weight (56, 57), produced predominantly *via* oxidative phosphorylation in
490 the mitochondria and, to a lesser extent, by glycolysis (58). Therefore, mitochondrial
491 health is critical for the proper functioning of the heart. A plethora of substrate are used
492 to produce ATP, including FA, glucose, lactate, and ketones (33, 59) and substrate
493 selection depends largely on substrate availability, oxygen concentration and myocardial

494 workload (60). Under normal conditions, the heart relies predominantly (~60-90%) on FA
495 oxidation to fuel ATP production, whereas the remaining ~10-40% of ATP is derived from
496 pyruvate oxidation (61). Metabolic flexibility (the capacity of the healthy heart to shift
497 between different substrates to ensure a continuous output of energy) is established as
498 a crucial feature of cardiac energy metabolism (62). Such flexibility is lost in CST-KO mice
499 because hearts in these mice show increased FA uptake and oxidation coupled with
500 decreased glucose uptake and oxidation; these changes have been reported in insulin-
501 resistant and diabetic rodents (63) and is a distinctive feature in obesity-associated
502 metabolic diseases in humans (64). Such metabolic inflexibility was reversed by
503 supplementation of CST-KO mice with CST, underscoring that CST is necessary and
504 sufficient for cardiometabolic homeostasis and flexibility.

505 As for how CST may regulate the cardiometabolic state, we found that
506 mitochondrial structure and function were altered in its absence and restored by
507 exogenous supplementation of CST. These findings are consistent with prior studies
508 showing that HTN is associated with decreased mitochondrial mass and density,
509 increased mitochondrial swelling, impaired energy production and the accelerated
510 formation of reactive oxygen species (ROS) (65). In addition, HTN rats display
511 mitochondrial fragmentation and increased ROS production (66).

512 In congruence with increased FA uptake in the setting of decreased mitochondrial
513 oxidative capacity, CST-KO mice displayed intramyocardial lipid droplets; such droplets
514 are normally found in an obese and diabetic heart (67, 68) and are known to trigger
515 mitochondrial dysfunction and energetic compromise, resulting in cardiac dysfunctions
516 (64, 69, 70). In addition, like a diabetic heart, myocardial insulin resistance (decreased
517 phosphorylation of AKT and GSK-3β) and impaired glucose utilization (decreased
518 glucose uptake and oxidation) in CST-KO mice resulted in a further increase in cardiac
519 FA uptake and accumulation of toxic lipid metabolites including triacylglycerol,
520 diacylglycerol, and ceramide (71, 72). Of note, inflammatory cytokines like TNFα induce
521 synthesis of ceramides, linking immune cells in induction of ceramide synthesis (73). We
522 have previously shown that CST markedly decreases triglyceride, FA and ceramides in
523 diet-induced obese (DIO) liver and improves insulin sensitivity in CST-KO and DIO mice
524 (23). CST supplementation in CST-KO mice results in the development of the following

525 phenotypes: (i) increased glucose uptake and metabolism, (ii) decreased FA uptake and
526 oxidation, (iii) decreased accumulation of lipid droplets, and finally, (iv) decreased
527 mitophagy, thereby underscoring the crucial roles that CST plays in improvement of
528 cardiac metabolism and function.
529
530 **Neuro-adrenergic overdrive-induced HTN and immunoendocrine regulation of BP.**
531 Existing literature reveals heightened SNA in white coat syndrome and borderline
532 hypertensive subjects (74), and the magnitude of the elevation of SNA is related to the
533 magnitude of HTN (75). Like humans, SHR shows reduced cardiac parasympathetic
534 nerve activity, elevated SNA and increased NA release (76). Here, we found neuro-
535 adrenergic overdrive-induced HTN in CST-KO mice. Augmented SNA in HTN is known
536 to activate both myeloid cells and T cells (5), and primary HTN shows increased
537 circulating concentration of proinflammatory cytokines such as TNFα and IL6 (77). To our
538 knowledge, the present study is the first to demonstrate increased infiltration of
539 macrophages in the adrenal medulla concomitant with increased secretion of
540 catecholamines and the consequent development of HTN in CST-KO mice, which were
541 normalized after CST supplementation. These findings imply that CST regulates BP
542 through a novel immunoendocrine regulation of catecholamine secretion.
543
544 We conclude that the anti-hypertensive effects of CST are mediated at least partly via
545 CST's anti-inflammatory actions, since without CST, macrophages are more reactive,
546 infiltrate the heart, and alter the ultrastructure, physiologic makeup, and molecular
547 makeup of the myocardium. Additionally, the data implicate CST as a key mediator of the
548 observed crosstalk between systemic and cardiac inflammation in HTN and acts as a
549 central mediator of cardiovascular homeostasis *via* a complex immunoendocrine axis.
550
551

552 **Material and Methods**

553

554 **Mice**. To generate CST-KO mice, we selectively targeted to eliminate the 63 bp CST encoding
555 segment from Exon VII of the *Chga* gene. The general cloning strategy involved PCR and
556 subcloning into pBluescript. We introduced a diphtheria toxin sequence to serve as a negative
557 selection at the 3'-end of the construct that would enrich (by ~5-fold) positive clones after
558 transfection of the targeted construct into ES cells by electroporation. For positive selection by
559 G418 we have introduced a Neo cassette flanked by FRT (*Flp* recognition target) site. PCR
560 screening of CST-KO mice are shown in **Fig. S1.**
561 Male WT and CST-KO (20-24 weeks old) with a mixed genetic background (50%
562 129svJ/50% C57BL/6) or in C57BL/6 background were studied. Since CgA is overexpressed in
563 patients with hypertension, especially hypertensive men, and CgA predicted catecholamine
564 secretion (78) we used only male mice in this study. Further studies will look into female mice.
565 Mice were kept in a 12 hr dark/light cycle and fed a normal chow diet (NCD: 13.5% calorie from
566 fat; LabDiet 5001, Lab Supply, Fort Worth, TX).

567

568 **Protein analysis by immunoblotting.** Left ventricles were homogenized in a buffer containing
569 phosphatase and protease inhibitors, as previously described (79). Homogenates were subjected
570 to SDS-PAGE and immunoblotted. Primary antibodies for phosphorylated and total AKT and
571 GSK-3β were from Cell Signaling Technology (Danvers, MA); mouse monoclonal mAb 5A8
572 ($hCgA_{R47-L57}$) antibody and rabbit polyclonal C-terminal CST pAb CT-CST ($hCgA_{P368-R373}$) (80)
573 were generously provided by Angelo Corti (IRCCS San Raffaele Scientific Institute, Milan, Italy).

574

575 **Echocardiography.** Echocardiography was performed as previously described (81). Briefly, adult
576 age-matched WT and CST-KO mice were anesthetized with 5% isoflurane and maintained with
577 0.5% isoflurane during the entire procedure. Vevo 2100 ultrasound system (FUJIFILM
578 VisualSonics Inc.) with a linear transducer 32-56MHz (MS550S) was used to capture the images
579 and videos. Heart rate, percentage fractional shortening (%FS), left ventricular (LV) internal
580 diameter at end-diastole (LVIDd) and end-systole (LVIDs), LV posterior wall thickness at end-
581 diastole (LVPWd) and interventricular septum thickness at end-diastole (IVSd) were measured
582 from the M-mode tracing.

583

584 **Non-invasive tail-cuff measurement of blood pressure**. Systolic blood pressure (SBP) was
585 measured using the mouse and rat tail cuff blood pressure (MRBP) System (IITC Life Sciences

586 Inc. Woodland Hills, CA). Mice were restrained in plexiglass tubes and heated to 34°C for 10-15
587 min in individual warming chambers prior to BP measurement. The tails were placed inside
588 inflatable cuffs with a photoelectric sensor that measured tail pulses. The SBP was measured
589 over 6 separate days with an average of two values per day.
590
591 **Determination of plasma CgA and CST.** Commercial mouse EIA kits were used to determine
592 CgA from two adrenal glands (CUSABIO Technology LLC, Houston, TX) and plasma (200 µl)
593 CST (RayBiotech Life, Peachtree Corners, GA) and followed according to the manufacturer's
594 protocol.
595
596 **Measurement of plasma cytokines.** Plasma cytokines (20 µl) were measured using U-PLEX
597 mouse cytokine assay kit (Meso Scale Diagnostics, Rockville, MD) via the manufacturer's
598 protocol.
599
600 **Transmission Electron Microscopy (TEM) and morphometric analysis.** To displace blood
601 and wash tissues before fixation, mice were cannulated through the apex of the heart and
602 perfused with a Ca^{2+} and Mg^{2+} free buffer composed of DPBS and 9.46 mM KCl (to arrest hearts
603 in diastole), as described previously (82). Fixation, embedding, sectioning and staining were done
604 following our previous publication (82). Grids were viewed using a JEOL JEM1400-plus TEM
605 (JEOL, Peabody, MA) and photographed using a Gatan OneView digital camera with 4k x 4k
606 resolution (Gatan, Pleasanton, CA). Morphometric analysis of glycogen granules and cristae
607 surface area were determined as described previously by us (80).
608
609 **Flow cytometry analysis**
610 Mouse heart perfusion was performed as previously described (50). Cardiac stromal cells were
611 stained with fluorescence-tagged antibodies to detect macrophages ($CD11b^{+}F4/80^{+}$). Data were
612 analyzed using FlowJo software.
613
614 **Tissue macrophage depletion study.**
615 To deplete tissue macrophages, mice were given clodronate liposomes (50 mg/kg body weight;
616 catalog F70101C-N, FormuMax, Sunnyvale, CA) every 3 days via intraperitoneal injection. Mice
617 treated with control liposomes were used as control.
618
619 **Bone marrow transplantation.**

620 To generate irradiated chimeras, 10-12 week old WT or CST-KO NCD recipient mice received a
621 lethal dose of 10 Gy radiation, followed by tail vein injection of 2 x 10^6 bone marrow cells from
622 either WT or CST-KO NCD donor mice. After 16 weeks of bone marrow transplantation, all mice
623 were subjected to non-invasive tail-cuff measurement of BP.
624
625 **Microarrays.** Total RNA from left ventricular tissue from four CST-KO and age-matched WT mice
626 was isolated using a RNeasy Kit. RNA quality was assessed by using the Agilent Model 2100
627 Bioanalyzer. RNA was labeled and hybridized to a Nimblegen mouse 12-plex array. Array was
628 scanned on a GenePix 4000B scanner and data extracted using Arraystar 4. Raw data was
629 analyzed using a Bayesian variance modeling approach in VAMPIRE using a FDR of 0.05 (83).
630 Data were visualized using GeneSpring 14.5. Microarray data is available at GEO Accession
631 Number (GSE104071).
632
633 **Real Time PCR**
634 Total RNA from heart tissue was isolated using RNeasy Mini Kit and reverse-transcribed using
635 qScript cDNA synthesis kit. cDNA samples were amplified using PERFECTA SYBR FASTMIX L-
636 ROX 1250 and analyzed on an Applied Biosystems 7500 Fast Real-Time PCR system. All PCRs
637 were normalized to *Rplp0*, and relative expression levels were determined by the $\Delta\Delta C_t$ method.
638
639 ***In vivo* tissue glucose uptake and metabolism.** *In vivo* glucose uptake and production of
640 glucose-6-phosphate (G6P) and glycogen was assessed following a published protocol but using
641 double isotopes - ^{3}H-glucose and ^{14}C-2-deoxyglucose (2DG) as described previously by us (82).
642
643 ***In vivo* fatty acid incorporation and lipid extraction and oxidation.** A 100 µl solution of U-^{14}C-
644 palmitic acid-BSA complex (molar ration 2.5:1), containing 1 µCi and 250 µM palmitate was
645 injected per mouse. After 90 min, mice were sacrificed, blood was saved and tissues were
646 subjected to lipid extraction by Bligh and Dyer's adaptation (84) of Folch's original method (85).
647 Radioactivity in the lower chloroform layer was determined by measuring fatty acids in the
648 aqueous layer by determining acid soluble metabolites (ASM, representing fatty acid oxidation)
649 as described previously by us (86).
650
651 **Determination of tissue glycogen.** Glycogen was extracted from the left ventricle by boiling with
652 30% KOH, precipitation by alcohol and determination with anthrone reagent (87).
653

654 **Langendorff perfused heart model.** Mice were anesthetized with sodium pentobarbital (50
655 mg/kg i.p.), the heart was excised and the aorta was cannulated for Langendorff perfusion of the
656 coronary circulation, as described previously (88). For the ischemic preconditioning (IPC) protocol
657 the stabilization period was followed by two cycles of ischemia (5 min, no pacing) and reperfusion
658 (5 min, pacing after 1 min re-perfusion).
659
660 **Measurement of catecholamines:** Mice were anesthetized by inhalation of isoflurane and blood
661 was collected from the heart in potassium-EDTA tubes. Adrenal and plasma catecholamines were
662 measured by ACQUITY UPLC H-Class System fitted with Atlantis dC18 column (100A, 3 µm, 3
663 mm x 100 mm) and connected to an electrochemical detector (ECD model 2465) (Waters Corp,
664 Milford, MA). The mobile phase (isocratic: 0.3 ml/min). consisted of phosphate-citrate buffer and
665 acetonitrile at 95:5 (vol/vol). An internal standard 3.4-dihydroxybenzylamine (DHBA 400 ng) was
666 added to the mixture of adrenal homogenate from one adrenal gland and 0.1N HCl (50 µl each).
667 While the injection volume for NE and EPI was 4 µl and the ECD was set at 50 nA, the injection
668 volume was 8 µl and the ECD was set at 2 nA. For determination of plasma catecholamines,
669 DHBA (2 ng) was added to 150 µl plasma (2 ng) and adsorbed with ~15 mg of activated aluminum
670 oxide for 10 min in a rotating shaker. After washing with 1 ml water adsorbed catecholamines
671 were eluted with 100 µl of 0.1N HCl. The injection volume was 10 µl and the ECD was set at 500
672 pA. The data were analyzed using Empower software (Waters Corp, Milford, MA). Catecholamine
673 levels were normalized with the recovery of the internal standard. Plasma catecholamines are
674 expressed as nM. Adrenal catecholamines are expressed as nmol/mg protein.
675
676 **Statistics.** Statistics were performed with SPSS Statistics (IBM Corp., Armonk, NY). Data were
677 analyzed either with a Repeated Measure (RM) 2x2 ANOVA, 2-way ANOVA, UNIANOVA, and
678 subjected to post-hoc tests and pairwise comparisons where appropriate. Additionally, we
679 performed unpaired student's t-test or Mann-Whitney U test depending on Shapiro-Wilk's test of
680 normality (with results corrected for Levene's test for Equality of Variances where appropriate).
681 All data are presented as mean ± SEM and significance was assumed when $p<0.05$.
682
683 **Study approval.** All studies with mice were approved by the UCSD and Veteran Affairs San
684 Diego Institutional Animal Care and Use Committees (IACUC) and conform to relevant National
685 Institutes of Health guidelines.
686

687 **Author contributions:**

688 W. Ying designed and generated CDN liposome and BMT data; and edited the MS. K.
689 Tang designed and generated qPCR, cytokine, CgA, CST, and catecholamine data, and
690 edited the MS. E. Avolio generated western blot data. J.M. Schilling generated ischemia
691 reperfusion and ischemic pre-conditioning data; and made statistical analyses. T. Pasqua
692 and G. Bandyopadhyay generated glucose and fatty acid uptake and oxidation data and
693 edited the MS. M.A. Liu generated blood pressure data and edited the MS. H. Cheng
694 made targeted *Chga* construct for generation of CST-KO mice. JZ and FS analyzed the
695 echocardiography data. S. Mahata generated qPCR data and edited the MS. S. Das
696 provided intellectual input in the analysis of the CST-KO immunophenotype. D.M. Roth
697 and H.H. Patel supervised ischemia reperfusion and ischemic pre-conditioning studies
698 and provided financial support for those studies. D. Sahoo analyzed and interpreted the
699 microarray dataset, generated heat map. N.J.G. Webster designed and generated
700 microarray data. P. Ghosh extensively edited the MS and Figures, interpreted
701 transcriptomic dataset, and provided crucial inputs on the overall organization of the MS
702 and Figures. S.K. Mahata conceived the idea, generated TEM data, supervised >90% of
703 the studies, analyzed the data and made the graphics with extensive inputs from P.G.,
704 wrote the MS with extensive inputs from P.G. and provided financial support (>95%).
705

706 **Acknowledgments:**

707 Supported by grants from the Veterans Affairs (I01 BX003934 to SKM; BX001963 to
708 HHP) and the National Institutes of Health (AI141630 to P.G, GM138385 to D.S and
709 HL091071, HL066941 to HHP).
710

711 **Disclosures:**

712 None
713

714 **Figure legends**

715

716 **Fig. 1. CST-KO mice have enlarged hearts.**

717 **(A) Schematic diagram** showing the cloning strategy for generating CST-KO mice. **(B)**
718 **Western blot** showing the presence of CgA in the LV of WT and CST-KO mice. **(C)**
719 **Western blot** showing the presence of CgA and CST. A rabbit polyclonal C-terminal CST
720 antibody detected a truncated CgA (CgA_{1-373}) in the WT mice but not in CST-KO mice,
721 confirming the deletion of CST domain. **(D). Graph** displays adrenal CgA content (n=12)**.**
722 **(E) Graph** displays plasma CST level (n=6). **(F&G) Representative echocardiograms**
723 from the left ventricle of age-matched male WT (n=12) and CST-KO (n=13) mice showing
724 increased posterior wall thickness (shown by white arrow) in CST-KO mice. **(H) Bar**
725 **graph** showing posterior wall thickness (n=12-13). **(I) Bar graphs** displaying
726 interventricular septal thickness (n=12-13). **(J) Weight** of wet heart (n=16). **(K&L) Size** of
727 the wet heart**. (M) Systolic BP** (n=12) in WT and CST-KO mice. DTA, diphtheria toxin;
728 FRT, *Flp* recognition target. The data were analyzed by unpaired t test using GraphPad
729 Prism software version 8.2. ***$p<0.001$.

730

731

732 **Fig. 2. CST-KO mice are hypertensive, display systemic and cardiac inflammation;**
733 **all phenotypes are reversed by exogenous CST (2 μg/g body weight for 3 weeks).**
734 **(A) Schematic diagram** showing the interventional studies. **(B) Plasma CST** after saline
735 or CST treatment (n=6). **(C) Plasma cytokines** in WT and CST-KO mice (n=8). **(D) RT-**
736 **qPCR data** showing steady-state mRNA levels of anti-inflammatory cytokines in LV
737 (n=8). **(E) RT-qPCR data** showing steady-state mRNA levels of proinflammatory
738 cytokines in LV (n=8). The data were analyzed either by unpaired t test or 2-way ANOVA
739 followed by Tukey's multiple comparison test. Ns, not significant; *$p<0.05$; **$p<0.01$;
740 ***$p<0.001$.
741
742

743 **Fig. 3. Macrophages are key mediators of the proinflammatory cardiovascular**
744 **phenotypes in the CST-KO mice.**
745 **(A) Schematic diagram** showing the interventional studies. **(B) SBP** after saline or CST
746 treatment. **(C, F&G) Ultrastructural demonstration** of macrophages in WT and CST-
747 KO heart (n=4). **(C) Saline-treated** WT and CST-KO heart. **(D) FACS data** showing
748 macrophage population in CST-KO heart (n=3). **(E) Bar graph** showing $CD45^+$
749 leukocytes in CST-KO mice. **(F) CST-treated** WT and CST-KO heart. **(G) CDN-treated**
750 WT and CST-KO heart. **(H) SBP** after depletion of macrophages by CDN (n=8). **(I) SBP**
751 after BMT into irradiated mice (n=8). **(J) Plasma CST** in BMT mice (n=6). The data were
752 analyzed either by unpaired t test or 2-way ANOVA followed by Tukey's multiple
753 comparison test. Col, collagen; IFM, intermyofibrillar mitochondria; MyoN, myocyte
754 nucleus; Mϕ, macrophage; ns, not significant; SL, sarcolemma; SSM, sub-sarcolemmal
755 mitochondria; ZD, Z disc. *$p<0.05$; **$p<0.01$; ***$p<0.001$.
756
757

758 **Fig. 4. Analysis of cardiac transcripts in CST-KO mice reveal defects in the core**
759 **myocardial functions.**
760 **(A) Gene array data** showing differential expression of genes (log2) in WT and CST-KO
761 mice (n=5). **(B) RT-qPCR data** validating gene array data (n=6). (**C**) **Expression of**
762 **sarcomere genes** in WT and CST-KO mice (n=6)**. (F) Expression of mitochondrial**
763 **genes** in WT and CST-KO mice (n=6). The data were analyzed by 2-way ANOVA
764 followed by Tukey's multiple comparison test. Ns, not significant; *p<0.05; **p<0.01;
765 ***p<0.001.
766
767

768 **Fig. 5. CST-KO mice display an altered cardiometabolic phenotype and insulin**
769 **resistance**
770 **(A) 2DG uptake, G6P formation and utilization** 90 min after 2DG injection (n=6). **(B)**
771 **Relative expression of genes** involved in glucose metabolism (n=6). **(C) FA uptake and**
772 **oxidation** (acid soluble metabolite: ASM) 90 min after injection of FA (n=6). (**D**) **Relative**
773 **expression of genes** involved in fat metabolism (n=6). **(E) Cardiac glycogen** level in
774 WT and CST-KO mice (n=6). **(F) Morphometric analyses** of glycogen granules. **(G)**
775 Ultrastructural demonstration of glycogen granules (GG) in LV of WT and CST-KO mice.
776 **(H) Representative LV immunoblots** of AKT and GSK-3β in fasting (12 hr) mice (n=4).
777 **(I&J) Densitometric** values of immunoblots: **(I)** AKT and **(J)** GSK-3β. The data were
778 analyzed by 2-way ANOVA followed by Tukey's multiple comparison test. SSM,
779 subsarcolemmal mitochondria; Ns, not significant; *p<0.05; **p<0.01; ***p<0.001.
780
781

782 **Fig. 6. CST-KO mice display altered mitochondrial morphology**
783 **Transmission Electron Microscopic (TEM) images showing mitochondria and**
784 **cristae (n=4). (A-D) Low magnification micrographs** showing sub-sarcolemmal
785 mitochondria (SSM). Mitophagy (Mp) is shown in saline-treated CST-KO mice **(C),** which
786 was abolished after CST treatment **(D). (E-H) High magnification micrographs** showing
787 SSM in saline-treated **(E&G)** and CST-treated **(F&H)** WT and CST-KO mice. **(I-L) Low**
788 **magnification micrographs** showing intermyofibrillar mitochondria (IFM) in WT and
789 CST-KO mice. Lipid droplets (LD) are seen juxtaposed to IFM in saline-treated CST-KO
790 mice **(K). (M-P) High magnification micrographs** showing IFM in WT and CST-KO
791 mice. **(Q) High magnification IFM** showing LD. **(R) High magnification SSM** showing
792 mitophagy (Mp). **(S) Morphometric data** showing cristae surface area. The data were
793 analyzed by 2-way ANOVA followed by Tukey's multiple comparison test.EDCS, electron
794 dense contact site; LD, lipid droplet; MyoN, myocyte nucleus; Ns, not significant; SL,
795 sarcolemma; ZD, Z-disc; *$p<0.05$.
796
797

798 **Fig. 7. CST-KO mice display inflamed adrenal medulla and altered catecholamine**
799 **secretion**
800 **(A) TEM micrographs of the adrenal medulla (n=4).** Low magnification micrographs
801 showing resident macrophage in WT mice and resident plus infiltrated macrophages in
802 CST-KO mice. (**B) Adrenal catecholamines** in WT and CST-KO mice (n=12). **(C)**
803 **Plasma catecholamines** in WT and CST-KO mice (n=12). **(D) High magnification**
804 **micrographs** showing chromaffin granules (CG) in the adrenal medulla. Docked CGs are
805 abundant in CST-KO mice. (**E**) **High magnification micrographs** showing splanchnico-
806 adrenomedullary synapse with clear acetylcholine vesicles (AChV) and dense core
807 peptidergic vesicles (PdV). The data were analyzed by 2-way ANOVA followed by
808 Tukey's multiple comparison test.AT, axon terminal; CC, chromaffin cell; CG, chromaffin
809 granule; GJ, gap junction; Mϕ, macrophage; ns, not significant; PM, plasma membrane;
810 *p<0.05; **p<0.01; ***p<0.001.
811
812

813 **Fig. 8. Summary or findings and working model.**

814 Schematic showing the major conclusions from the current work and its relevance to
815 human cardiovascular health and HTN. CST maintains cardiac homeostasis and prevents
816 HTN and cardiac remodeling (hypertrophy and fibrosis) *via* two major mechanisms (red
817 lines) - First, it exerts an anti-inflammatory action *via* its effect on macrophage processes
818 and polarization. Second, it exerts a negative feedback loop on catecholamine secretion
819 from chromaffin cells (6, 89, 90). In the absence of CST, plasma catecholamines are
820 elevated and macrophages become reactive in phenotype. While the former results in
821 HTN, the latter causes inflammation in the adrenals and heart. Macrophage infiltration in
822 the heart and local secretion of cytokines by activated macrophages result in altered
823 myocardial ultrastructure, bioenergetics, cardiometabolic shift, insulin resistance, and
824 core myocardial functions, e.g., BP and cardioprotection by IPC. In doing so, CST acts
825 as a central mediator of cardiovascular homeostasis *via* a complex immunoendocrine
826 axis.

827

828 **References**

829

830 1. Bromfield S, and Muntner P. High blood pressure: the leading global burden of
831 disease risk factor and the need for worldwide prevention programs. *Curr*
832 *Hypertens Rep.* 2013;15(3):134-6.
833 2. Goldstein DS. Plasma catecholamines and essential hypertension. An analytical
834 review. *Hypertension.* 1983;5(1):86-99.
835 3. Floras JS. Epinephrine and the genesis of hypertension. *Hypertension.*
836 1992;19(1):1-18.
837 4. Coffman TM. Under pressure: the search for the essential mechanisms of
838 hypertension. *Nat Med.* 2011;17(11):1402-9.
839 5. Norlander AE, Madhur MS, and Harrison DG. The immunology of hypertension. *J*
840 *Exp Med.* 2018;215(1):21-33.
841 6. Mahata SK, O'Connor DT, Mahata M, Yoo SH, Taupenot L, Wu H, et al. Novel
842 autocrine feedback control of catecholamine release. A discrete chromogranin A
843 fragment is a noncompetitive nicotinic cholinergic antagonist. *J Clin Invest.*
844 1997;100(6):1623-33.
845 7. Winkler H, and Fischer-Colbrie R. The chromogranins A and B: the first 25 years
846 and future perspectives. *Neuroscience.* 1992;49(3):497-528.
847 8. Bartolomucci A, Possenti R, Mahata SK, Fischer-Colbrie R, Loh YP, and Salton
848 SR. The extended granin family: structure, function, and biomedical implications.
849 *Endocr Rev.* 2011;32(6):755-97.
850 9. O'Connor DT, Zhu G, Rao F, Taupenot L, Fung MM, Das M, et al. Heritability and
851 genome-wide linkage in US and australian twins identify novel genomic regions
852 controlling chromogranin a: implications for secretion and blood pressure.
853 *Circulation.* 2008;118(3):247-57.
854 10. O'Connor DT, Takiyyuddin MA, Printz MP, Dinh TQ, Barbosa JA, Rozansky DJ, et
855 al. Catecholamine storage vesicle protein expression in genetic hypertension.
856 *Blood Press.* 1999;8(5-6):285-95.
857 11. O'Connor DT, Kailasam MT, Kennedy BP, Ziegler MG, Yanaihara N, and Parmer
858 RJ. Early decline in the catecholamine release-inhibitory peptide catestatin in
859 humans at genetic risk of hypertension. *J Hypertens.* 2002;20:1335-45.
860 12. Wen G, Mahata SK, Cadman P, Mahata M, Ghosh S, Mahapatra NR, et al. Both
861 rare and common polymorphisms contribute functional variation at CHGA, a
862 regulator of catecholamine physiology. *Am J Hum Genet.* 2004;74(2):197-207.
863 13. Rao F, Wen G, Gayen JR, Das M, Vaingankar SM, Rana BK, et al. Catecholamine
864 release-inhibitory peptide catestatin (chromogranin A(352-372)): naturally
865 occurring amino acid variant Gly364Ser causes profound changes in human
866 autonomic activity and alters risk for hypertension. *Circulation.* 2007;115(17):2271-
867 81.
868 14. Angelone T, Quintieri AM, Brar BK, Limchaiyawat PT, Tota B, Mahata SK, et al.
869 The antihypertensive chromogranin a peptide catestatin acts as a novel
870 endocrine/paracrine modulator of cardiac inotropism and lusitropism.
871 *Endocrinology.* 2008;149(10):4780-93.

15. Kiranmayi M, Chirasani VR, Allu PK, Subramanian L, Martelli EE, Sahu BS, et al. Catestatin Gly364Ser Variant Alters Systemic Blood Pressure and the Risk for Hypertension in Human Populations via Endothelial Nitric Oxide Pathway. *Hypertension.* 2016.
16. Ottesen AH, Carlson CR, Louch WE, Dahl MB, Sandbu RA, Johansen RF, et al. Glycosylated Chromogranin A in Heart Failure: Implications for Processing and Cardiomyocyte Calcium Homeostasis. *Circ Heart Fail.* 2017;10(2).
17. Mahapatra NR, O'Connor DT, Vaingankar SM, Hikim AP, Mahata M, Ray S, et al. Hypertension from targeted ablation of chromogranin A can be rescued by the human ortholog. *J Clin Invest.* 2005;115(7):1942-52.
18. Mahata SK, and Corti A. Chromogranin A and its fragments in cardiovascular, immunometabolic, and cancer regulation. *Ann N Y Acad Sci.* 2019;1455(1):34-58.
19. Eliakim-Raz N, Prokupetz A, Gordon B, Shochat T, and Grossman A. Interventricular Septum and Posterior Wall Thickness Are Associated With Higher Systolic Blood Pressure. *J Clin Hypertens (Greenwich).* 2016;18(7):703-6.
20. Lim PO, Donnan PT, and MacDonald TM. Blood pressure determinants of left ventricular wall thickness and mass index in hypertension: comparing office, ambulatory and exercise blood pressures. *J Hum Hypertens.* 2001;15(9):627-33.
21. Perrone-Filardi P, Coca A, Galderisi M, Paolillo S, Alpendurada F, de Simone G, et al. Non-invasive cardiovascular imaging for evaluating subclinical target organ damage in hypertensive patients: A consensus paper from the European Association of Cardiovascular Imaging (EACVI), the European Society of Cardiology Council on Hypertension, and the European Society of Hypertension (ESH). *Eur Heart J Cardiovasc Imaging.* 2017;18(9):945-60.
22. Perrone-Filardi P, Coca A, Galderisi M, Paolillo S, Alpendurada F, de Simone G, et al. Noninvasive cardiovascular imaging for evaluating subclinical target organ damage in hypertensive patients: a consensus article from the European Association of Cardiovascular Imaging, the European Society of Cardiology Council on Hypertension and the European Society of Hypertension. *J Hypertens.* 2017;35(9):1727-41.
23. Ying W, Mahata S, Bandyopadhyay GK, Zhou Z, Wollam J, Vu J, et al. Catestatin Inhibits Obesity-Induced Macrophage Infiltration and Inflammation in the Liver and Suppresses Hepatic Glucose Production, Leading to Improved Insulin Sensitivity. *Diabetes.* 2018;67(5):841-8.
24. Kojima M, Ozawa N, Mori Y, Takahashi Y, Watanabe-Kominato K, Shirai R, et al. Catestatin Prevents Macrophage-Driven Atherosclerosis but Not Arterial Injury-Induced Neointimal Hyperplasia. *Thromb Haemost.* 2018;118(1):182-94.
25. Chen H, Liu D, Ge L, Wang T, Ma Z, Han Y, et al. Catestatin prevents endothelial inflammation and promotes thrombus resolution in acute pulmonary embolism in mice. *Biosci Rep.* 2019;39(11).
26. Zivkovic PM, Matetic A, Tadin Hadjina I, Rusic D, Vilovic M, Supe-Domic D, et al. Serum Catestatin Levels and Arterial Stiffness Parameters Are Increased in Patients with Inflammatory Bowel Disease. *J Clin Med.* 2020;9(3).
27. Avolio E, Mahata SK, Mantuano E, Mele M, Alo R, Facciolo RM, et al. Antihypertensive and neuroprotective effects of catestatin in spontaneously

917 hypertensive rats: Interaction with GABAergic transmission in amygdala and
918 brainstem. *Neuroscience.* 2014;270:48-57.
919 28. Granger JP. An emerging role for inflammatory cytokines in hypertension. *Am J*
920 *Physiol Heart Circ Physiol.* 2006;290(3):H923-4.
921 29. Brands MW, Banes-Berceli AK, Inscho EW, Al-Azawi H, Allen AJ, and Labazi H.
922 Interleukin 6 knockout prevents angiotensin II hypertension: role of renal
923 vasoconstriction and janus kinase 2/signal transducer and activator of transcription
924 3 activation. *Hypertension.* 2010;56(5):879-84.
925 30. Ishimitsu T, Uehara Y, Numabe A, Tsukada H, Ogawa Y, and Yagi S.
926 Antihypertensive effect of interleukin-2 in salt-sensitive Dahl rats. *Hypertension.*
927 1994;23(1):68-73.
928 31. Tuttle RS, and Boppana DP. Antihypertensive effect of interleukin-2. *Hypertension.*
929 1990;15(1):89-94.
930 32. Viel EC, Lemarie CA, Benkirane K, Paradis P, and Schiffrin EL. Immune regulation
931 and vascular inflammation in genetic hypertension. *Am J Physiol Heart Circ*
932 *Physiol.* 2010;298(3):H938-44.
933 33. Ritterhoff J, and Tian R. Metabolism in cardiomyopathy: every substrate matters.
934 *Cardiovasc Res.* 2017;113(4):411-21.
935 34. Stanley WC, Lopaschuk GD, Hall JL, and McCormack JG. Regulation of
936 myocardial carbohydrate metabolism under normal and ischaemic conditions.
937 Potential for pharmacological interventions. *Cardiovasc Res.* 1997;33(2):243-57.
938 35. Mishra PK, Ying W, Nandi SS, Bandyopadhyay GK, Patel KK, and Mahata SK.
939 Diabetic Cardiomyopathy: An Immunometabolic Perspective. *Front Endocrinol*
940 *(Lausanne).* 2017;8:72.
941 36. Sokolowska E, and Blachnio-Zabielska A. The Role of Ceramides in Insulin
942 Resistance. *Front Endocrinol (Lausanne).* 2019;10:577.
943 37. Dasgupta A, Bandyopadhyay GK, Ray I, Bandyopadhyay K, Chowdhury N, De RK,
944 et al. Catestatin improves insulin sensitivity by attenuating endoplasmic reticulum
945 stress: In vivo and in silico validation. *Comput Struct Biotechnol J.* 2020;18:464-
946 81.
947 38. Mehta MM, Weinberg SE, and Chandel NS. Mitochondrial control of immunity:
948 beyond ATP. *Nat Rev Immunol.* 2017;17(10):608-20.
949 39. Cogliati S, Frezza C, Soriano ME, Varanita T, Quintana-Cabrera R, Corrado M, et
950 al. Mitochondrial cristae shape determines respiratory chain supercomplexes
951 assembly and respiratory efficiency. *Cell.* 2013;155(1):160-71.
952 40. Hollander JM, Thapa D, and Shepherd DL. Physiological and structural differences
953 in spatially distinct subpopulations of cardiac mitochondria: influence of cardiac
954 pathologies. *Am J Physiol Heart Circ Physiol.* 2014;307(1):H1-14.
955 41. Crochemore C, Mekki M, Corbiere C, Karoui A, Noel R, Vendeville C, et al.
956 Subsarcolemmal and interfibrillar mitochondria display distinct superoxide
957 production profiles. *Free Radic Res.* 2015;49(3):331-7.
958 42. Westermeier F, Navarro-Marquez M, Lopez-Crisosto C, Bravo-Sagua R, Quiroga
959 C, Bustamante M, et al. Defective insulin signaling and mitochondrial dynamics in
960 diabetic cardiomyopathy. *Biochim Biophys Acta.* 2015;1853(5):1113-8.

43. Delbridge LMD, Mellor KM, Taylor DJ, and Gottlieb RA. Myocardial stress and autophagy: mechanisms and potential therapies. *Nat Rev Cardiol.* 2017;14(7):412-25.
44. Corssmit EP, Heijligenberg R, Endert E, Ackermans MT, Sauerwein HP, and Romijn JA. Endocrine and metabolic effects of interferon-alpha in humans. *J Clin Endocrinol Metab.* 1996;81(9):3265-9.
45. Kannan H, Tanaka Y, Kunitake T, Ueta Y, Hayashida Y, and Yamashita H. Activation of sympathetic outflow by recombinant human interleukin-1 beta in conscious rats. *Am J Physiol.* 1996;270(2 Pt 2):R479-85.
46. Darling G, Goldstein DS, Stull R, Gorschboth CM, and Norton JA. Tumor necrosis factor: immune endocrine interaction. *Surgery.* 1989;106(6):1155-60.
47. Lavine KJ, Epelman S, Uchida K, Weber KJ, Nichols CG, Schilling JD, et al. Distinct macrophage lineages contribute to disparate patterns of cardiac recovery and remodeling in the neonatal and adult heart. *Proc Natl Acad Sci U S A.* 2014;111(45):16029-34.
48. Heo GS, Kopecky B, Sultan D, Ou M, Feng G, Bajpai G, et al. Molecular Imaging Visualizes Recruitment of Inflammatory Monocytes and Macrophages to the Injured Heart. *Circ Res.* 2019;124(6):881-90.
49. Bajpai G, Bredemeyer A, Li W, Zaitsev K, Koenig AL, Lokshina I, et al. Tissue Resident CCR2- and CCR2+ Cardiac Macrophages Differentially Orchestrate Monocyte Recruitment and Fate Specification Following Myocardial Injury. *Circ Res.* 2019;124(2):263-78.
50. Hulsmans M, Sager HB, Roh JD, Valero-Munoz M, Houstis NE, Iwamoto Y, et al. Cardiac macrophages promote diastolic dysfunction. *J Exp Med.* 2018;215(2):423-40.
51. Heidt T, Courties G, Dutta P, Sager HB, Sebas M, Iwamoto Y, et al. Differential contribution of monocytes to heart macrophages in steady-state and after myocardial infarction. *Circ Res.* 2014;115(2):284-95.
52. Mann DL. Innate immunity and the failing heart: the cytokine hypothesis revisited. *Circ Res.* 2015;116(7):1254-68.
53. Bergman MR, Kao RH, McCune SA, and Holycross BJ. Myocardial tumor necrosis factor-alpha secretion in hypertensive and heart failure-prone rats. *Am J Physiol.* 1999;277(2):H543-50.
54. Levine B, Kalman J, Mayer L, Fillit HM, and Packer M. Elevated circulating levels of tumor necrosis factor in severe chronic heart failure. *N Engl J Med.* 1990;323(4):236-41.
55. Ashrafian H, Frenneaux MP, and Opie LH. Metabolic mechanisms in heart failure. *Circulation.* 2007;116(4):434-48.
56. Mootha VK, Arai AE, and Balaban RS. Maximum oxidative phosphorylation capacity of the mammalian heart. *Am J Physiol.* 1997;272(2 Pt 2):H769-75.
57. Neubauer S. The failing heart--an engine out of fuel. *N Engl J Med.* 2007;356(11):1140-51.
58. Ingwall JS. Energy metabolism in heart failure and remodelling. *Cardiovasc Res.* 2009;81(3):412-9.
59. Neely JR, Rovetto MJ, and Oram JF. Myocardial utilization of carbohydrate and lipids. *Prog Cardiovasc Dis.* 1972;15(3):289-329.

1007 60. Marelli-Berg FM, and Aksentijevic D. Immunometabolic cross-talk in the inflamed
1008 heart. *Cell Stress.* 2019;3(8):240-66.
1009 61. Stanley WC, Recchia FA, and Lopaschuk GD. Myocardial substrate metabolism in
1010 the normal and failing heart. *Physiol Rev.* 2005;85(3):1093-129.
1011 62. Bertero E, and Maack C. Metabolic remodelling in heart failure. *Nat Rev Cardiol.*
1012 2018;15(8):457-70.
1013 63. Mazumder PK, O'Neill BT, Roberts MW, Buchanan J, Yun UJ, Cooksey RC, et al.
1014 Impaired cardiac efficiency and increased fatty acid oxidation in insulin-resistant
1015 ob/ob mouse hearts. *Diabetes.* 2004;53(9):2366-74.
1016 64. Fukushima A, and Lopaschuk GD. Cardiac fatty acid oxidation in heart failure
1017 associated with obesity and diabetes. *Biochim Biophys Acta.* 2016;1861(10):1525-
1018 34.
1019 65. Touyz RM. Reactive oxygen species, vascular oxidative stress, and redox
1020 signaling in hypertension: what is the clinical significance? *Hypertension.*
1021 2004;44(3):248-52.
1022 66. Rimbaud S, Ruiz M, Piquereau J, Mateo P, Fortin D, Veksler V, et al. Resveratrol
1023 improves survival, hemodynamics and energetics in a rat model of hypertension
1024 leading to heart failure. *PLoS One.* 2011;6(10):e26391.
1025 67. Lopaschuk GD, Ussher JR, Folmes CD, Jaswal JS, and Stanley WC. Myocardial
1026 fatty acid metabolism in health and disease. *Physiol Rev.* 2010;90(1):207-58.
1027 68. Zlobine I, Gopal K, and Ussher JR. Lipotoxicity in obesity and diabetes-related
1028 cardiac dysfunction. *Biochim Biophys Acta.* 2016;1861(10):1555-68.
1029 69. D'Souza K, Nzirorera C, and Kienesberger PC. Lipid metabolism and signaling in
1030 cardiac lipotoxicity. *Biochim Biophys Acta.* 2016;1861(10):1513-24.
1031 70. Unger RH. Lipotoxic diseases. *Annu Rev Med.* 2002;53:319-36.
1032 71. Peterson LR, Herrero P, Schechtman KB, Racette SB, Waggoner AD, Kisrieva-
1033 Ware Z, et al. Effect of obesity and insulin resistance on myocardial substrate
1034 metabolism and efficiency in young women. *Circulation.* 2004;109(18):2191-6.
1035 72. Gray S, and Kim JK. New insights into insulin resistance in the diabetic heart.
1036 *Trends in endocrinology and metabolism: TEM.* 2011;22(10):394-403.
1037 73. Smith EL, and Schuchman EH. The unexpected role of acid sphingomyelinase in
1038 cell death and the pathophysiology of common diseases. *FASEB J.*
1039 2008;22(10):3419-31.
1040 74. Anderson EA, Sinkey CA, Lawton WJ, and Mark AL. Elevated sympathetic nerve
1041 activity in borderline hypertensive humans. Evidence from direct intraneural
1042 recordings. *Hypertension.* 1989;14(2):177-83.
1043 75. Grassi G. Role of the sympathetic nervous system in human hypertension. *J*
1044 *Hypertens.* 1998;16(12 Pt 2):1979-87.
1045 76. Judy WV, and Farrell SK. Arterial baroreceptor reflex control of sympathetic nerve
1046 activity in the spontaneously hypertensive rat. *Hypertension.* 1979;1(6):605-14.
1047 77. Libby P, Ridker PM, and Maseri A. Inflammation and atherosclerosis. *Circulation.*
1048 2002;105(9):1135-43.
1049 78. Chen Y, Rao F, Rodriguez-Flores JL, Mahata M, Fung MM, Stridsberg M, et al.
1050 Naturally occurring human genetic variation in the 3'-untranslated region of the
1051 secretory protein chromogranin A is associated with autonomic blood pressure

1052 regulation and hypertension in a sex-dependent fashion. *J Am Coll Cardiol.*
1053 2008;52(18):1468-81.
1054 79. Bandyopadhyay GK, Vu CU, Gentile S, Lee H, Biswas N, Chi NW, et al. Catestatin
1055 (chromogranin A(352-372)) and novel effects on mobilization of fat from adipose
1056 tissue through regulation of adrenergic and leptin signaling. *J Biol Chem.*
1057 2012;287(27):23141-51.
1058 80. Sahu BS, Mahata S, Bandyopadhyay K, Mahata M, Avolio E, Pasqua T, et al.
1059 Catestatin regulates vesicular quanta through modulation of cholinergic and
1060 peptidergic (PACAPergic) stimulation in PC12 cells. *Cell Tissue Res.*
1061 2019;376(1):51-70.
1062 81. Sheikh F, Raskin A, Chu PH, Lange S, Domenighetti AA, Zheng M, et al. An FHL1-
1063 containing complex within the cardiomyocyte sarcomere mediates hypertrophic
1064 biomechanical stress responses in mice. *J Clin Invest.* 2008;118(12):3870-80.
1065 82. Pasqua T, Mahata S, Bandyopadhyay GK, Biswas A, Perkins GA, Sinha-Hikim
1066 AP, et al. Impact of Chromogranin A deficiency on catecholamine storage,
1067 catecholamine granule morphology and chromaffin cell energy metabolism in vivo.
1068 *Cell Tissue Res.* 2016;363(3):693-712.
1069 83. Hsiao A, Worrall DS, Olefsky JM, and Subramaniam S. Variance-modeled
1070 posterior inference of microarray data: detecting gene-expression changes in 3T3-
1071 L1 adipocytes. *Bioinformatics.* 2004;20(17):3108-27.
1072 84. Bligh EG, and Dyer WJ. A rapid method of total lipid extraction and purification.
1073 *Can J Biochem Physiol.* 1959;37(8):911-7.
1074 85. Folch J, Lees M, and Sloane Stanley GH. A simple method for the isolation and
1075 purification of total lipides from animal tissues. *J Biol Chem.* 1957;226(1):497-509.
1076 86. Tang K, Pasqua T, Biswas A, Mahata S, Tang J, Tang A, et al. Muscle injury,
1077 impaired muscle function and insulin resistance in Chromogranin A-knockout mice.
1078 *J Endocrinol.* 2017;232(2):137-53.
1079 87. Carroll NV, Longley RW, and Roe JH. The determination of glycogen in liver and
1080 muscle by use of anthrone reagent. *J Biol Chem.* 1956;220(2):583-93.
1081 88. Headrick JP, Willems L, Ashton KJ, Holmgren K, Peart J, and Matherne GP.
1082 Ischaemic tolerance in aged mouse myocardium: the role of adenosine and effects
1083 of A1 adenosine receptor overexpression. *J Physiol.* 2003;549(Pt 3):823-33.
1084 89. Mahata SK, Mahata M, Wakade AR, and O'Connor DT. Primary structure and
1085 function of the catecholamine release inhibitory peptide catestatin (chromogranin
1086 A344-364): Identification of amino acid residues crucial for activity. *Mol Endocrinol.*
1087 2000;14(10):1525-35.
1088 90. Mahata SK, Mahapatra NR, Mahata M, Wang TC, Kennedy BP, Ziegler MG, et al.
1089 Catecholamine secretory vesicle stimulus-transcription coupling in vivo.
1090 Demonstration by a novel transgenic promoter/photoprotein reporter and inhibition
1091 of secretion and transcription by the chromogranin A fragment catestatin. *J Biol*
1092 *Chem.* 2003;278:32058-67.
1093

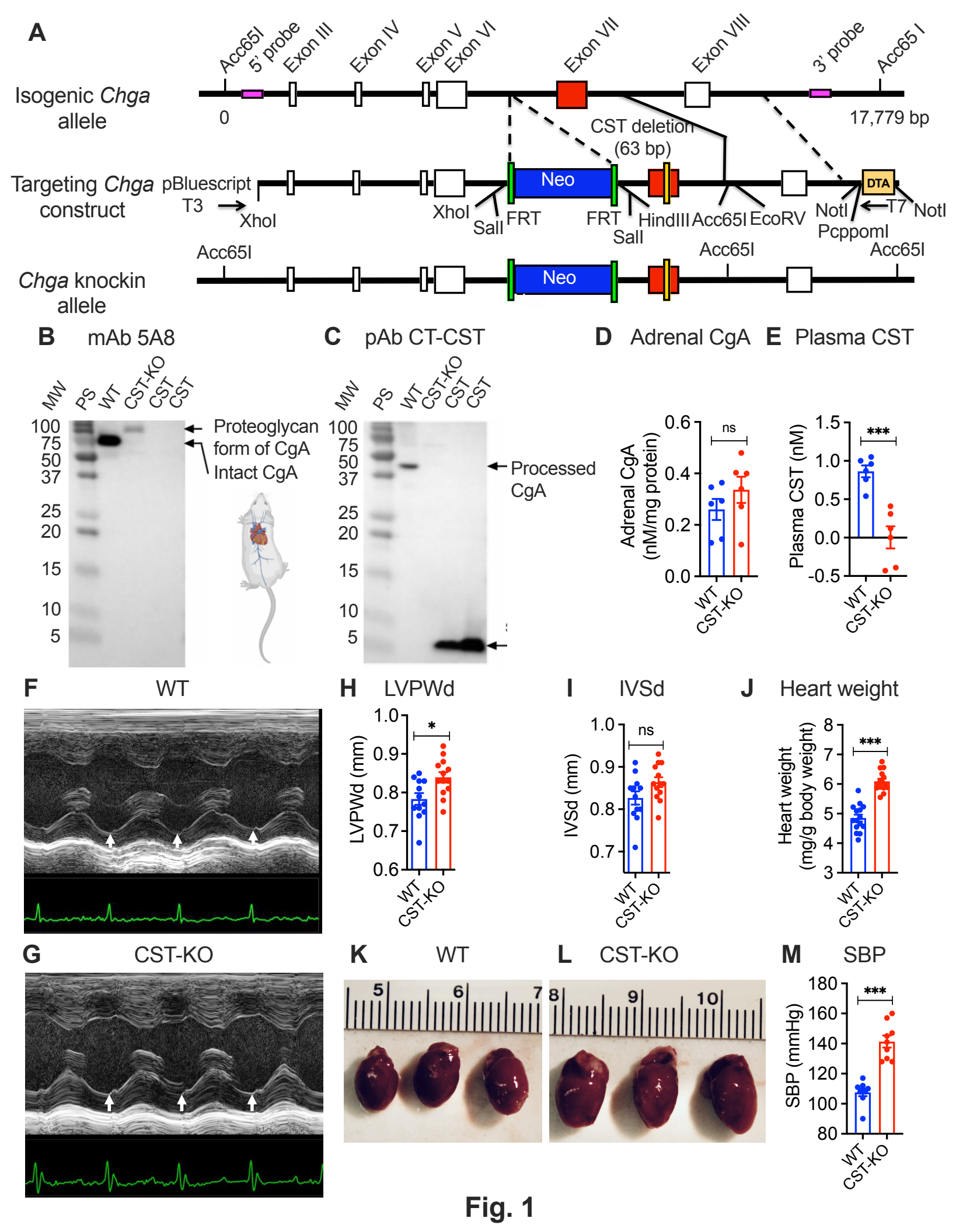
A
Isogenic Chga allele
Acc65I
5' probe
Exon III
Exon IV
Exon V
Exon VI
Exon VII
Exon VIII
3' probe
Acc65 I
0
17,779 bp
CST deletion (63 bp)
Targeting Chga construct
pBluescript
T3
XhoI
XhoI
SalI
FRT
Neo
FRT
SalI
HindIII
Acc65I
EcoRV
NotI
PcppomI
T7
NotI
DTA
Chga knockin allele
Acc65I
Neo
Acc65I
Acc65I
B mAb 5A8
MW
PS
WT
CST-KO
CST
CST
100
75
50
37
25
20
15
10
5
Proteoglycan form of CgA
Intact CgA
C pAb CT-CST
Processed CgA
D Adrenal CgA
Adrenal CgA (nM/mg protein)
ns
WT
CST-KO
E Plasma CST
Plasma CST (nM)
***
F WT
G CST-KO
H LVPWd
LVPWd (mm)
*
I IVSd
IVSd (mm)
ns
J Heart weight
Heart weight (mg/g body weight)
***
K WT
L CST-KO
M SBP
SBP (mmHg)
***

Fig. 1

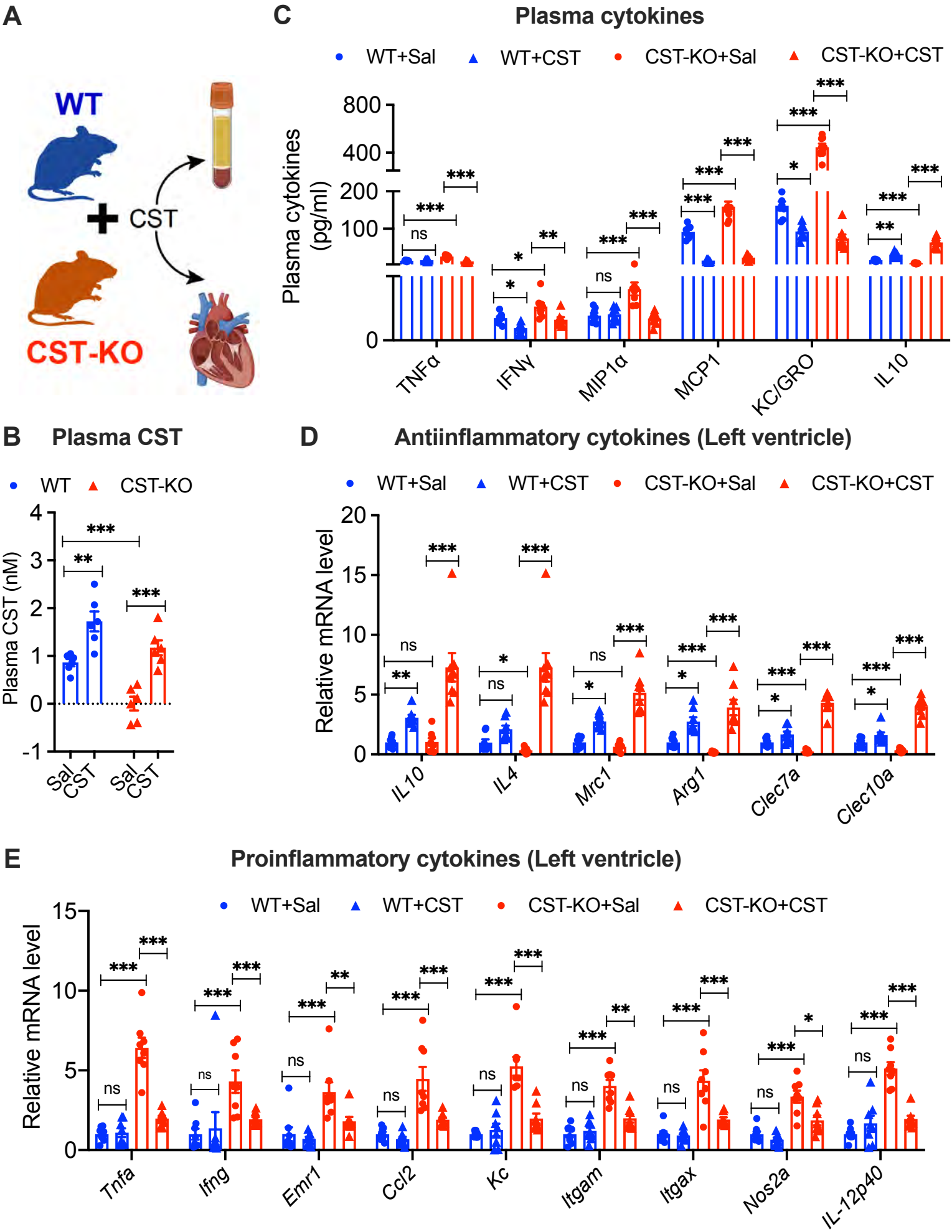
A
WT
CST
CST-KO
B
Plasma CST
WT
CST-KO
Plasma CST (nM)
Sal
CST
Sal
CST
C
Plasma cytokines
WT+Sal
WT+CST
CST-KO+Sal
CST-KO+CST
Plasma cytokines (pg/ml)
TNFα
IFNγ
MIP1α
MCP1
KC/GRO
IL10
D
Antiinflammatory cytokines (Left ventricle)
Relative mRNA level
IL10
IL4
Mrc1
Arg1
Clec7a
Clec10a
E
Proinflammatory cytokines (Left ventricle)
Relative mRNA level
Tnfa
Ifng
Emr1
Ccl2
Kc
Itgam
Itgax
Nos2a
IL-12p40

Fig. 2

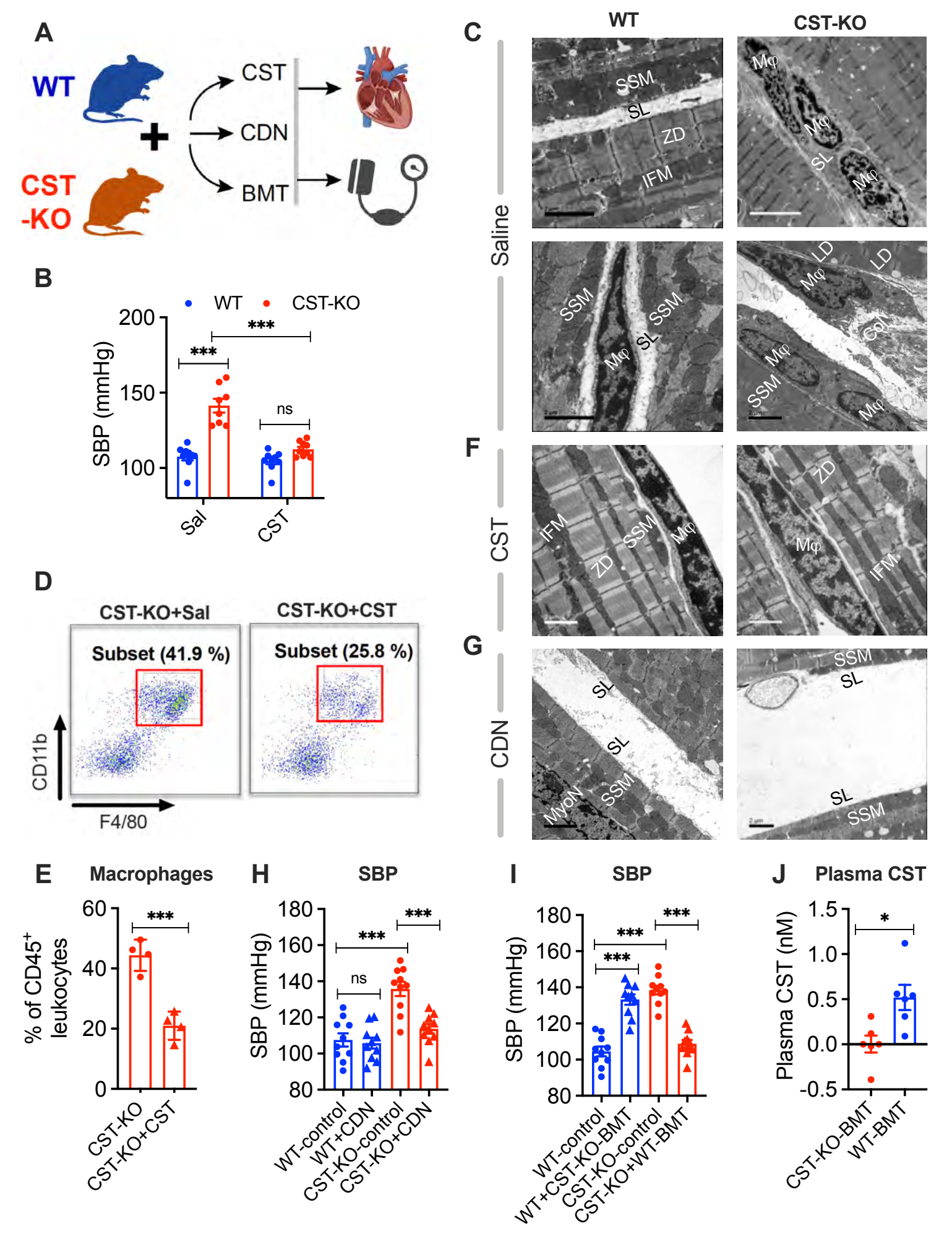
A
WT
CST
-KO
CST
CDN
BMT
B
WT
CST-KO
SBP (mmHg)
200
150
100
***
***
ns
Sal
CST
C
WT
CST-KO
Saline
SSM
SL
ZD
IFM
Mφ
LD
Col
F
CST
ZD
IFM
SSM
Mφ
G
CDN
SL
SSM
MyoN
D
CST-KO+Sal
CST-KO+CST
Subset (41.9 %)
Subset (25.8 %)
CD11b
F4/80
E
Macrophages
% of CD45+ leukocytes
60
40
20
0
***
CST-KO
CST-KO+CST
H
SBP
SBP (mmHg)
180
160
140
120
100
80
***
***
ns
WT-control
WT+CDN
CST-KO-control
CST-KO+CDN
I
SBP
SBP (mmHg)
***
***
***
WT-control
WT+CST-KO-BMT
CST-KO-control
CST-KO+WT-BMT
J
Plasma CST
Plasma CST (nM)
1.5
1.0
0.5
0.0
-0.5
*
CST-KO-BMT
WT-BMT

Fig. 3

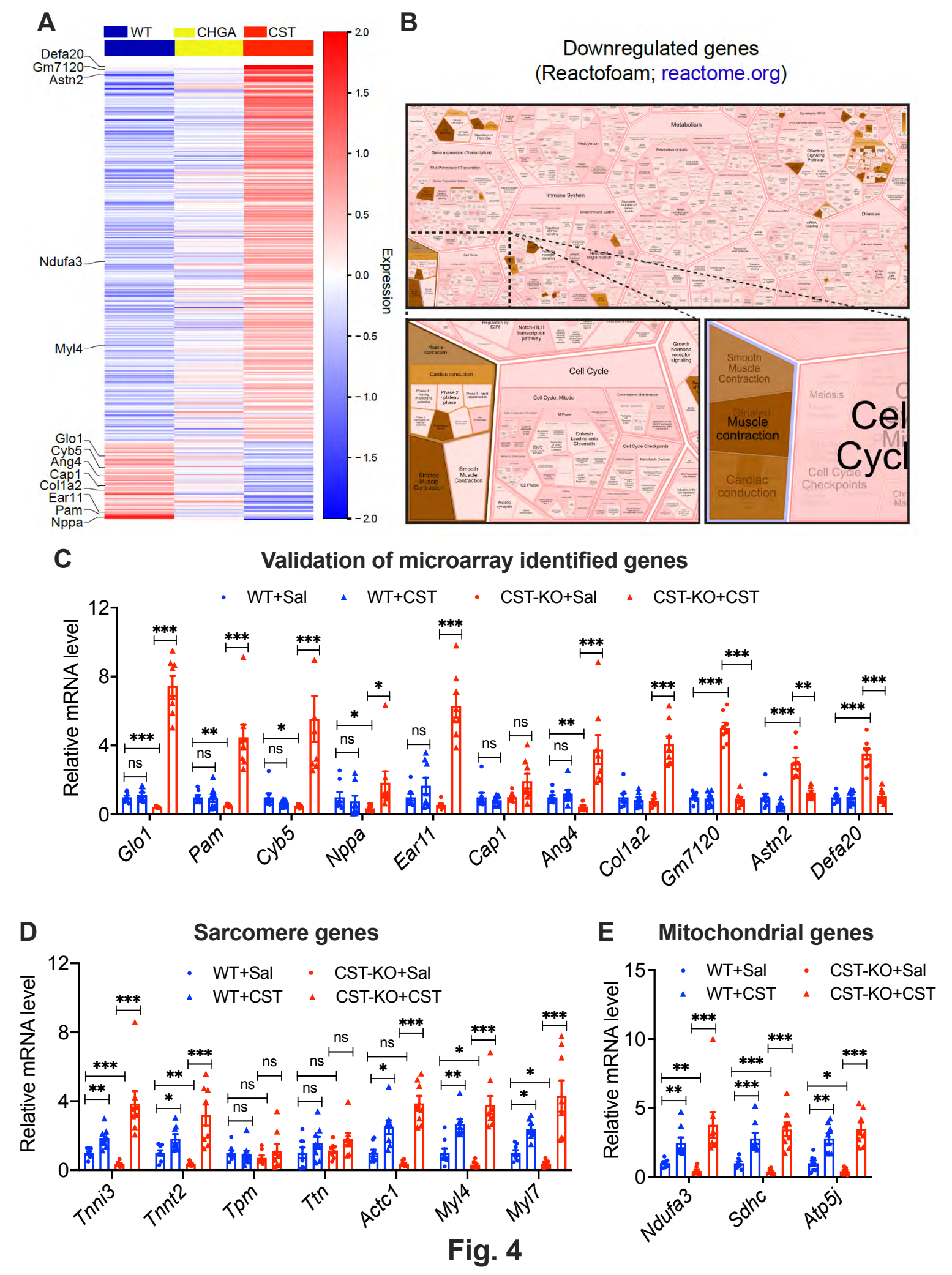
A
WT
CHGA
CST
Defa20
Gm7120
Astn2
Ndufa3
Myl4
Glo1
Cyb5
Ang4
Cap1
Col1a2
Ear11
Pam
Nppa
Expression
2.0
1.5
1.0
0.5
0.0
−0.5
−1.0
−1.5
−2.0
B
Downregulated genes
(Reactofoam; reactome.org)
Metabolism
Gene expression (Transcription)
Immune System
Disease
Cell Cycle
Muscle contraction
Cardiac conduction
Smooth Muscle Contraction
Striated Muscle Contraction
Cell Cycle, Mitotic
Cell Cycle Checkpoints
Meiosis
C
Validation of microarray identified genes
WT+Sal
WT+CST
CST-KO+Sal
CST-KO+CST
Relative mRNA level
Glo1
Pam
Cyb5
Nppa
Ear11
Cap1
Ang4
Col1a2
Gm7120
Astn2
Defa20
D
Sarcomere genes
Tnni3
Tnnt2
Tpm
Ttn
Actc1
Myl4
Myl7
E
Mitochondrial genes
Ndufa3
Sdhc
Atp5j

Fig. 4

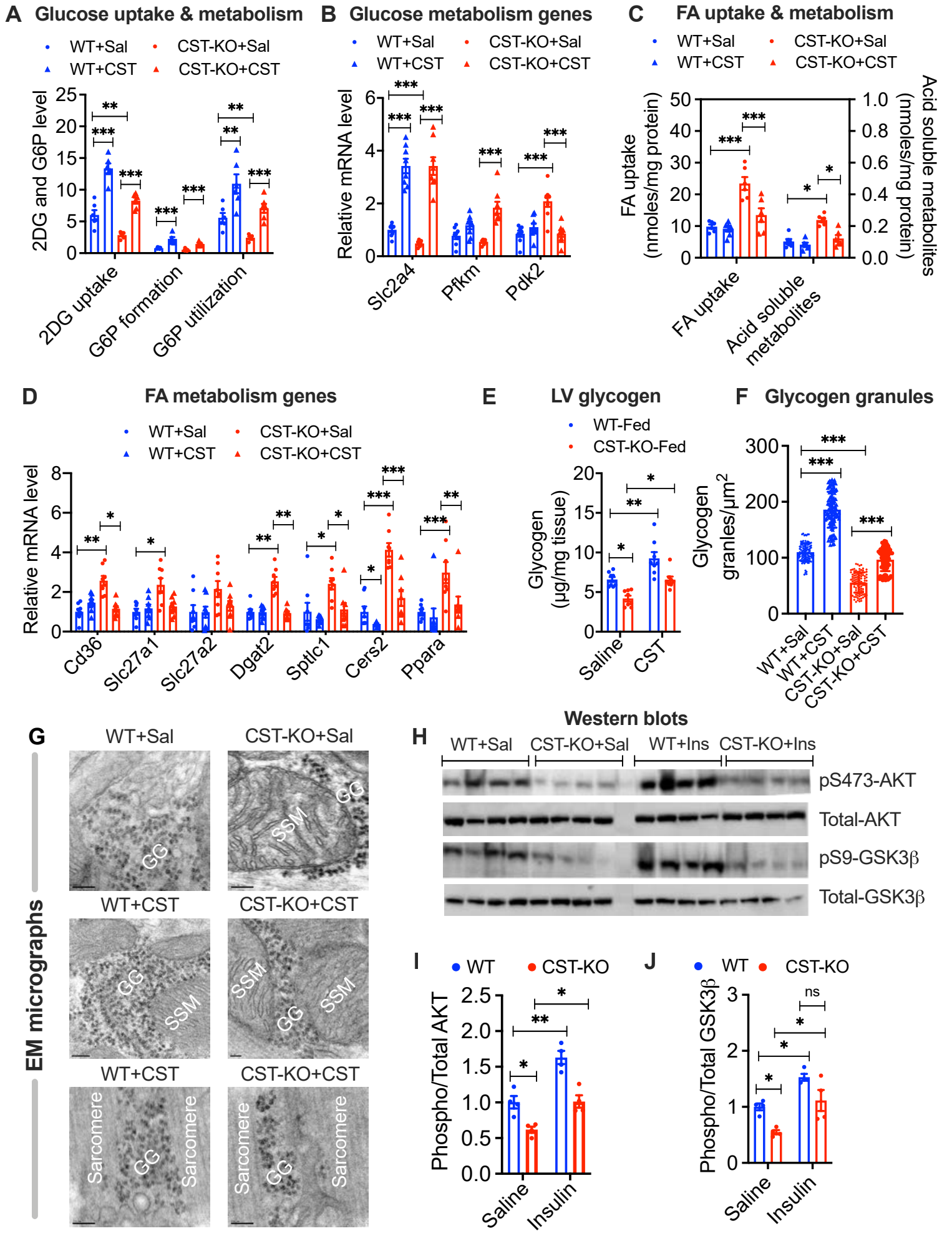
A Glucose uptake & metabolism
WT+Sal
CST-KO+Sal
WT+CST
CST-KO+CST
2DG and G6P level
2DG uptake
G6P formation
G6P utilization
B Glucose metabolism genes
Relative mRNA level
Slc2a4
Pfkm
Pdk2
C FA uptake & metabolism
FA uptake (nmoles/mg protein)
Acid soluble metabolites (nmoles/mg protein)
FA uptake
Acid soluble metabolites
D FA metabolism genes
Relative mRNA level
Cd36
Slc27a1
Slc27a2
Dgat2
Sptlc1
Cers2
Ppara
E LV glycogen
WT-Fed
CST-KO-Fed
Glycogen (μg/mg tissue)
Saline
CST
F Glycogen granules
Glycogen granles/μm2
WT+Sal
WT+CST
CST-KO+Sal
CST-KO+CST
G
EM micrographs
WT+Sal
CST-KO+Sal
WT+CST
CST-KO+CST
GG
SSM
Sarcomere
H
Western blots
WT+Sal
CST-KO+Sal
WT+Ins
CST-KO+Ins
pS473-AKT
Total-AKT
pS9-GSK3β
Total-GSK3β
I
WT
CST-KO
Phospho/Total AKT
Saline
Insulin
J
WT
CST-KO
Phospho/Total GSK3β
ns
Saline
Insulin

Fig. 5

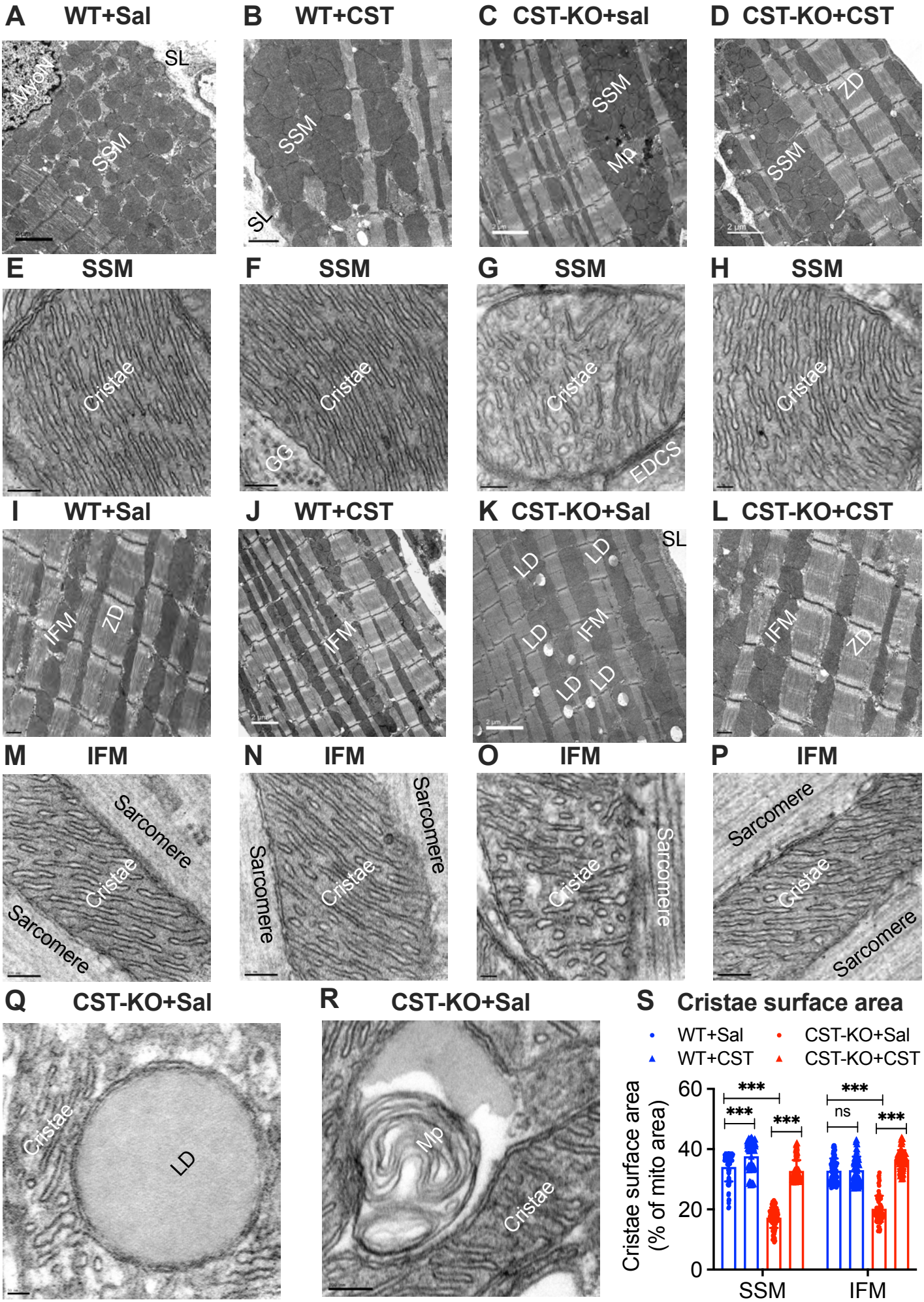
A WT+Sal
B WT+CST
C CST-KO+sal
D CST-KO+CST
MyoN
SL
SSM
Mp
ZD
E SSM
F SSM
G SSM
H SSM
Cristae
GG
EDCS
I WT+Sal
J WT+CST
K CST-KO+Sal
L CST-KO+CST
IFM
LD
M IFM
N IFM
O IFM
P IFM
Sarcomere
Q CST-KO+Sal
R CST-KO+Sal
S Cristae surface area
WT+Sal
WT+CST
CST-KO+Sal
CST-KO+CST
Cristae surface area
(% of mito area)
60
40
20
0
***
ns
SSM
IFM

Fig. 6

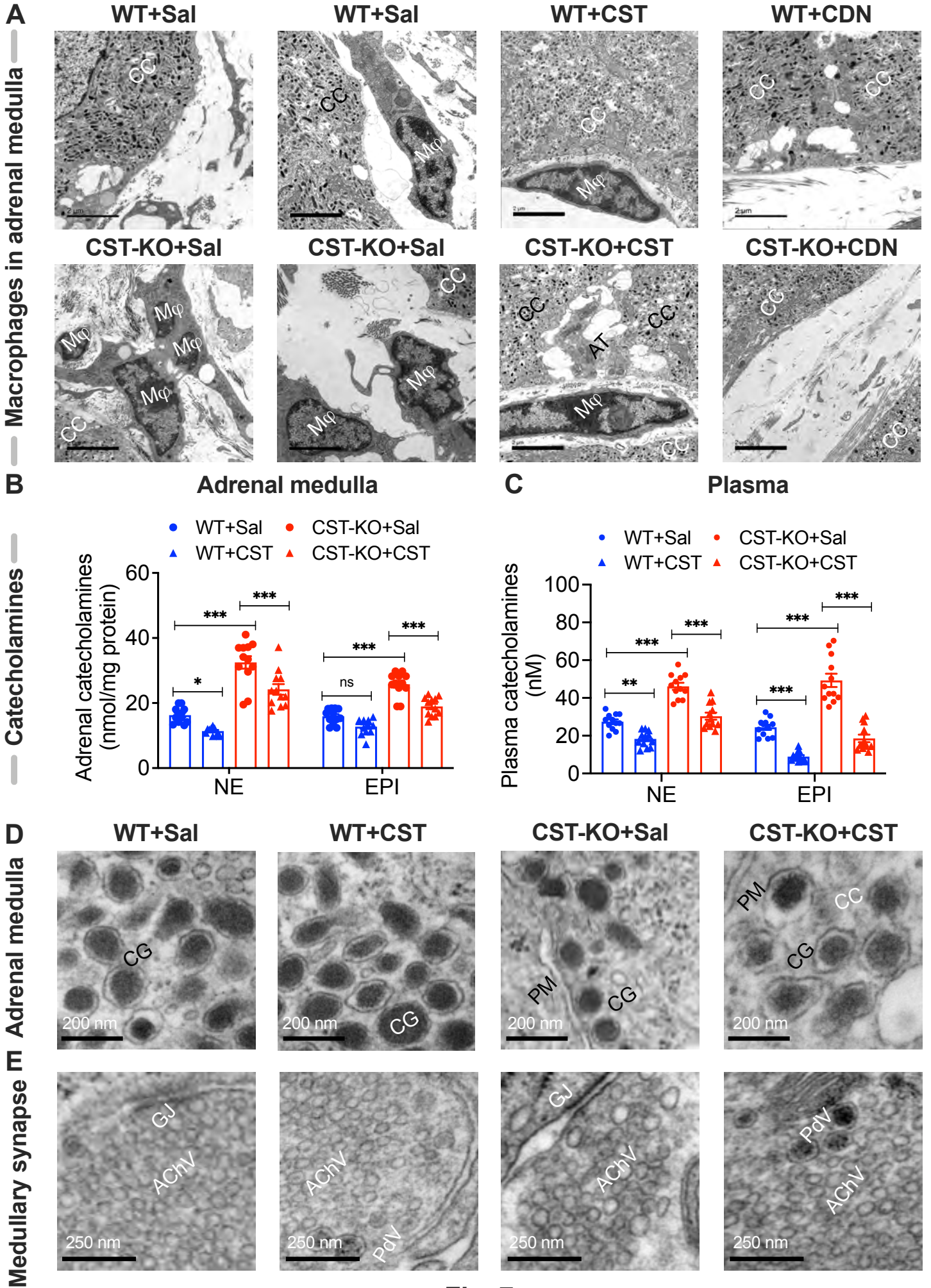
A
Macrophages in adrenal medulla
WT+Sal
WT+Sal
WT+CST
WT+CDN
CST-KO+Sal
CST-KO+Sal
CST-KO+CST
CST-KO+CDN
CC
Mφ
AT
B
Adrenal medulla
Catecholamines
WT+Sal
CST-KO+Sal
WT+CST
CST-KO+CST
Adrenal catecholamines (nmol/mg protein)
NE
EPI
ns
C
Plasma
Plasma catecholamines (nM)
D
Adrenal medulla
Medullary synapse
CG
PM
GJ
AChV
PdV
200 nm
250 nm

Fig. 7

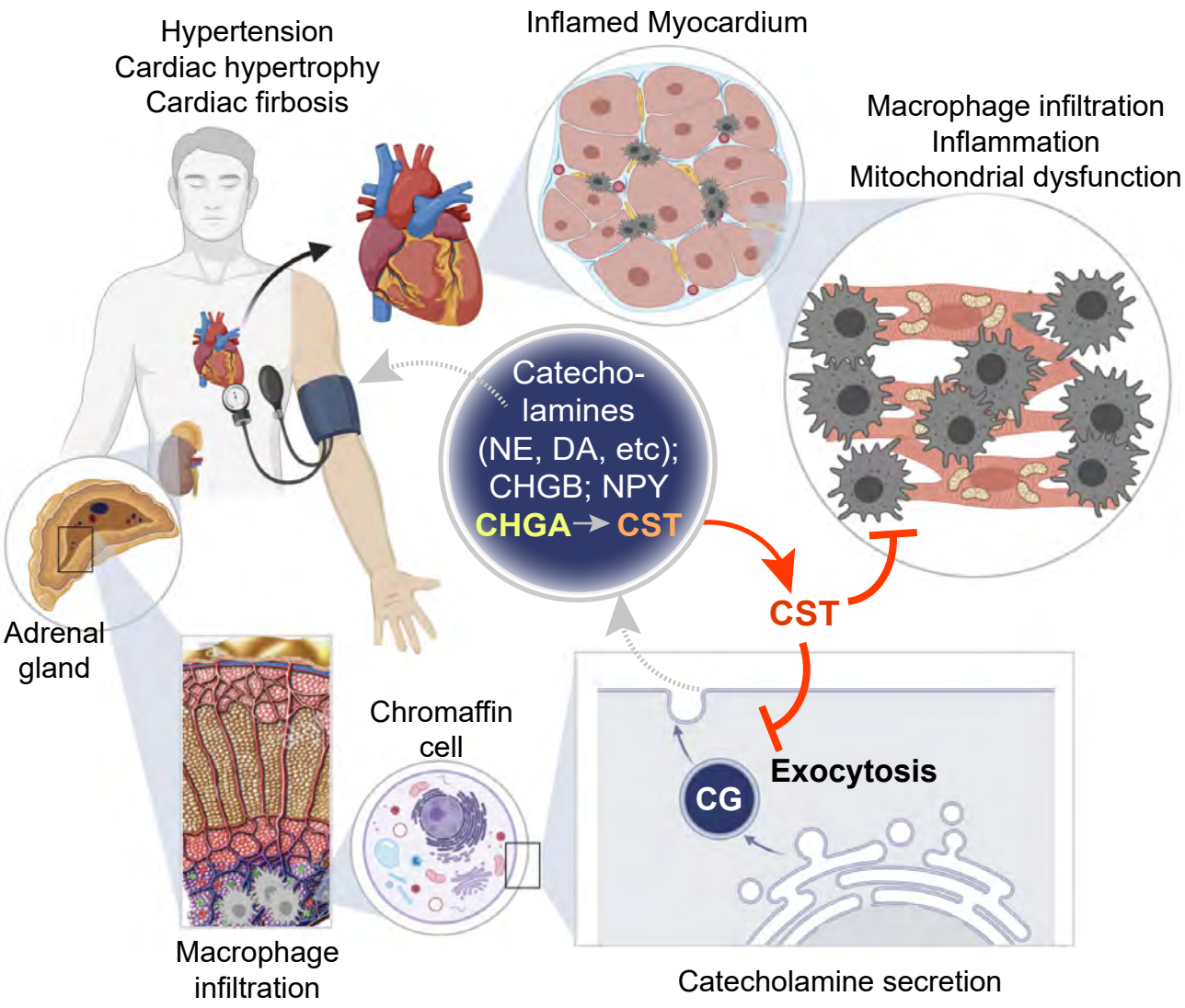
Hypertension
Cardiac hypertrophy
Cardiac firbosis
Inflamed Myocardium
Macrophage infiltration
Inflammation
Mitochondrial dysfunction
Catecho-
lamines
(NE, DA, etc);
CHGB; NPY
CHGA→ CST
CST
Adrenal
gland
Chromaffin
cell
CG
Exocytosis
Macrophage
infiltration
Catecholamine secretion

Fig 8.